

1 **Advantages of assimilating multi-spectral satellite retrievals of atmospheric composition: A**  
2 **demonstration using MOPITT CO products**

3  
4 **Wenfu Tang<sup>1</sup>, Benjamin Gaubert<sup>1</sup>, Louisa K. Emmons<sup>1</sup>, Daniel Ziskin<sup>1</sup>, Debbie Mao<sup>1</sup>, David**  
5 **P. Edwards<sup>1</sup>, Avelino F. Arellano<sup>2</sup>, Kevin Raeder<sup>3</sup>, Jeffrey L. Anderson<sup>3</sup>, and Helen M.**  
6 **Worden<sup>1</sup>**  
7

8 <sup>1</sup>Atmospheric Chemistry Observations & Modeling Laboratory, National Center for Atmospheric  
9 Research, Boulder, CO, USA

10 <sup>2</sup>Dept. of Hydrology and Atmospheric Sciences, University of Arizona, Tucson, AZ, USA

11 <sup>3</sup>Computational and Information Systems Laboratory, National Center for Atmospheric Research,  
12 Boulder, CO, USA

13  
14 Correspondence: Wenfu Tang ([wenfut@ucar.edu](mailto:wenfut@ucar.edu))  
15

16 **Abstract**

17 The Measurements Of Pollution In The Troposphere (MOPITT) is an ideal instrument to  
18 understand the impact of (1) assimilating multispectral/joint retrievals versus single-spectral  
19 products, (2) assimilating satellite profile products versus column products, and (3) assimilating  
20 multispectral/joint retrievals versus assimilating individual products separately. We use the  
21 Community Atmosphere Model with chemistry with the Data Assimilation Research Testbed  
22 (CAM-chem+DART) to assimilate different MOPITT CO products to address these three  
23 questions. Both anthropogenic and fire CO emissions are optimized in the data assimilation  
24 experiments. The results are compared with independent CO observations from TROPOspheric  
25 Monitoring Instrument (TROPOMI), the Total Carbon Column Observing Network (TCCON),  
26 NOAA Carbon Cycle Greenhouse Gases (CCGG) sites, In-service Aircraft for a Global Observing  
27 System (IAGOS), and Western wildfire Experiment for Cloud chemistry, Aerosol absorption and  
28 Nitrogen (WE-CAN). We find that (1) assimilating the MOPITT joint (multispectral Near-IR and  
29 Thermal-IR) column product leads to better model-observation agreement at and near the surface  
30 than assimilating the MOPITT Thermal-IR-only column retrieval. (2) Assimilating column  
31 products has a larger impact and improvement for background and large-scale CO compared to  
32 assimilating profile products due to vertical localization in profile assimilation. However, profile  
33 assimilation can out-perform column assimilations in fire-impacted regions and near the  
34 surface. (3) Assimilating multispectral/joint products results in similar or slightly better agreement  
35 with observations compared to assimilating the single-spectral products separately.  
36

37  
38 **1 Introduction**

39 With the increasing availability of satellite remote sensing instruments measuring  
40 atmospheric composition, there is potential to produce multispectral retrievals of several species,  
41 making use of thermal-infrared (TIR) and near-infrared (NIR) radiances from collocated  
42 instruments on the same satellite such as IASI (Infrared Atmospheric Sounding Interferometer)  
43 and GOME-2 (Global Ozone Monitoring Experiment-2) on the European MetOp satellites (Cuesta  
44 et al., 2013), or flying in close formation, such as on the NASA A-train and the NOAA's JPSS  
45 (Joint Polar Satellite System), e.g., OMI (Ozone Monitoring Instrument, Levelt et al., 2018), AIRS

46 (Atmospheric Infrared Sounder, Fu et al., 2018), OMPS (Ozone Mapping and Profiler Suite, Flynn  
 47 et al., 2014), TROPospheric Monitoring Instrument (TROPOMI, Veeffkind et al., 2012) and CrIS  
 48 (Cross-track Infrared Sounder, Fu et al., 2016). TIR retrievals use thermal contrast while NIR  
 49 retrievals use reflected solar radiance from the surface. Taking MOPITT as an example, the TIR  
 50 retrieval can provide vertical profiles with limited sensitivity to the surface while the NIR retrieval  
 51 only provide total column product with some sensitivity to the surface (Figure 1).

52 The multispectral products have shown considerable increases in the vertical sensitivity of  
 53 the retrievals for lowermost tropospheric ozone (O<sub>3</sub>) (e.g., Worden et al., 2007; Natraj et al., 2011;  
 54 Fu 2018), carbon monoxide (CO) (Worden et al., 2010; Fu et al., 2016) and methane (CH<sub>4</sub>)  
 55 (Schneider et al. 2022). Multispectral retrievals could be made using the co-located overpass made  
 56 by low earth orbit and geostationary satellite such as, e.g., Geostationary Interferometric Infrared  
 57 Sounder (GIIRS, Zeng et al., 2023), Geostationary Environment Monitoring Spectrometer  
 58 (GEMS, Kim et al., 2020), [Geostationary Extended Observations \(GeoXO; Kopacz et al., 2023\)](#)  
 59 and Tropospheric emissions: Monitoring of pollution (TEMPO, Chance et al., 2019). Table 1  
 60 shows the developed and potential multispectral products. It is important to understand the value  
 61 of assimilating a multispectral product versus assimilating a single-spectral range product, and the  
 62 value of assimilating a multispectral product versus separately assimilating single-spectral range  
 63 products that are used to retrieve the multispectral products.

64  
65

66 **Table 1.** Developed and potential multispectral satellite retrievals. Shown in the table are satellites,  
 67 their NIR and/or TIR spectral ranges (in μm), and potential chemical species from the multispectral  
 68 retrievals.

Morning Overpass	Afternoon Overpass	Geostationary
MOPITT (2.3 & 4.7)	AIRS (3.75–15.4) + OMI (0.27–0.5)	GIIRS (East Asia) (0.55–14.2) + TROPOMI (2.3–2.4)
(CO)	(O <sub>3</sub> )	(CO, O <sub>3</sub> )
IASI (3.6–15.5) + GOME2 (0.24–0.79) (O <sub>3</sub> )	TES (8.7–10.5) + OMI (0.27–0.5)	GEMS (East Asia) (0.3–0.5) + IASI (3.6–15.5)
	(O <sub>3</sub> )	(O <sub>3</sub> )
	GOSAT (0.75–15) + TES (8.7–10.5)	GEMS (East Asia) (0.3–0.5) + CrIS (3.9–15.4)
	(O <sub>3</sub> )	(O <sub>3</sub> )
	CrIS (3.9–15.4) + GOSAT-2 (0.3–14.3)	TEMPO (N. America) (0.29–0.74) + IASI (3.6–15.5)
	(CO, CH <sub>4</sub> )	(O <sub>3</sub> )
	CrIS (3.9–15.4) + TROPOMI (2.3–2.4)	TEMPO (N. America) (0.29–0.74) + CrIS (3.9–15.4)
	(CO, O <sub>3</sub> , CH <sub>4</sub> )	(O <sub>3</sub> )

69  
70

71 Total column observations of [O<sub>3</sub>](#), CO and [Nitrogen Dioxide \(NO<sub>2</sub>\)](#) are now routinely  
 72 assimilated in operational centers such as in the European Copernicus Atmosphere Monitoring  
 73 Service (CAMS) program at the European Centre for Medium-Range Weather Forecasts (Inness  
 74 et al., 2019; 2022) In addition, recently launched geostationary satellites such as GEMS and  
 75 TEMPO will provide column products at high temporal resolution. While the satellite profile  
 76 products are in general considered to contain more vertical information, it is important to  
 77 understand the impacts of assimilating column products versus assimilating profile products and  
 78 to understand what information is potentially missed by only assimilating column products. For  
 79 example, Jiang et al. (2017) compared emission updates following the assimilation of the

Deleted: An example of averaging kernels of the MOPITT TIR and NIR retrievals can be found in the Figure 2 of Worden et al. (2010).

Deleted: ozone

Deleted:

Formatted: Subscript

85 Measurements of Pollution in the Troposphere (MOPITT) lowermost surface profile, the  
86 tropospheric profile or the columns and identified errors indicative of model transport error  
87 impacts on emission estimates.

88 The MOPITT instrument onboard the NASA Terra satellite is an ideal instrument to  
89 address these three questions. MOPITT retrieves total column amounts and vertical profiles of CO  
90 using both thermal-infrared (TIR) and near-infrared (NIR) measurements. In addition, MOPITT  
91 also provides the multispectral TIR-NIR joint product, which has enhanced the sensitivity to near-  
92 surface CO (Deeter et al., 2011, 2013; Worden et al., 2010). By comparing the results of  
93 assimilating different combinations of MOPITT CO products, we will be able to address these two  
94 questions.

95 To conduct the data assimilation experiments, we use the Community Atmosphere Model  
96 with chemistry and the Data Assimilation Research Testbed (Anderson et al., 2009). CAM-  
97 chem+DART has been previously used to assimilate MOPITT profile products (Arellano et al.,  
98 2007; Barré et al., 2015; Gaubert et al., 2016, 2017, 2020, 2023). Here we present the first  
99 assimilation of MOPITT column products within CAM-chem+DART. This new capability also  
100 allows us to assimilate other satellite column products of CO and other chemical species in the  
101 future. Anthropogenic and fire emissions are optimized separately in the data assimilation  
102 experiments.

103 This paper aims to understand the impacts of (1) assimilating multispectral/joint products  
104 versus single-spectral products, (2) assimilating satellite profile products versus column products,  
105 and (3) assimilating multispectral/joint products versus assimilating individual products  
106 separately. The paper is organized as follows: Section 2 describes CAM-chem, DART, and  
107 methods, Section 3 describes datasets used for results evaluation, Section 4 presents data  
108 assimilation diagnostics, Section 5 shows comparisons between data assimilation results and  
109 independent observations, Section 6 discuss optimized emissions and CAM-chem simulations  
110 with updated emissions, Section 7 is discussion and Section 8 concludes the study.

## 114 Section 2: Methods and data

### 115 2.1 MOPITT products

116 The Measurements of Pollution in the Troposphere (MOPITT) instrument on board the  
117 NASA Terra satellite provides both thermal-infrared (TIR) and near-infrared (NIR) radiance  
118 measurements since March 2000 (Deeter et al., 2003). CO total column amounts and volume  
119 mixing ratio (VMR) profiles (10 vertical layers) are retrieved from the radiance measurements.  
120 TIR is used to retrieve MOPITT TIR CO total column product and MOPITT TIR CO vertical  
121 profile product; NIR is used to retrieve MOPITT NIR CO column product. Besides the TIR-only  
122 and NIR-only products, multispectral (JNT) products are also provided by MOPITT by jointly  
123 retrieving from TIR and NIR. JNT retrievals provide both MOPITT JNT CO total column product  
124 and MOPITT JNT CO vertical profile product. JNT products have enhanced the sensitivity to near-  
125 surface CO (Deeter et al., 2011, 2013; Worden et al., 2010). MOPITT products can be accessed  
126 through <https://search.earthdata.nasa.gov/search>. In this study, we assimilate daytime MOPITT  
127 version 9 products (Deeter et al., 2022) of TIR profile, TIR column, NIR column, JNT profile, and  
128 JNT column in our experiments.

129 We use the error-weighted average of the MOPITT data within  $1^{\circ} \times 1^{\circ}$  model grid and 6-  
130 hourly bin (i.e., super-observations). Averaged daily numbers of daytime total super-observations

Deleted: Measurements of Pollution in the Troposphere (MOPITT) ...

Deleted: results

134 from MOPITT TIR, NIR, and JNT products during July 16<sup>th</sup> 2018 to August 14<sup>th</sup> 2018 is shown  
135 in Figure 2. The NIR product only covers the land while TIR and JNT products cover the land and  
136 ocean. Over the ocean, the JNT product is the same as the TIR product (Worden et al., 2010).

137 Data assimilation requires observation errors associated with the quantity assimilated.  
138 MOPITT provides 3 types of uncertainties/errors: total error, measurement error, and smoothing  
139 error in the products. Total error includes both measurement error and smoothing error. Since our  
140 observation operators include the smoothing by the MOPITT averaging kernels and the prior  
141 profiles, we only use the measurement error rather than total error provided by MOPITT for both  
142 column and profile products as smoothing error is already addressed by observation operators in  
143 the system (Rodgers, 2000). Specifically, for MOPITT profile products, measurement error is  
144 provided by the variable "MeasurementErrorCovarianceMatrix" while for MOPITT column  
145 products, measurement error is provided by the variable second column of the  
146 "RetrievedCOTotalColumnDiagnosticsDay".

## 149 2.2 CAM-chem

150 The Community Earth System Model (CESM) is a global Earth system model that includes  
151 the atmosphere, land, ocean, and ice components (Danabasoglu et al., 2020). CAM-chem  
152 (Emmons et al., 2020; Tilmes et al., 2019) is a global chemistry-climate model as a configuration  
153 of CESM version 2.2 (<https://www2.acom.ucar.edu/gcm/cam-chem>). CAM-chem accounts for  
154 physical, chemical and dynamical processes with a spatial resolution of 1.25° in longitude and  
155 0.95° in latitude and 32 vertical layers with ~8 layers in boundary layer and ~10 layers in the free  
156 troposphere (Tang et al., 2023). We use the default MOZART-TS1 chemical mechanism, which  
157 includes comprehensive tropospheric and stratospheric chemistry with ~220 chemical species and  
158 528 reactions (Emmons et al., 2020). The aerosol scheme used is the four-mode version of the  
159 Modal Aerosol Module (MAM4; Liu et al., 2016).

160 We use CAMS-GLOB-ANT v5.1 inventory (Soulie et al., 2023) for anthropogenic  
161 emissions and FINNv2.4 (Wiedinmyer et al., 2023) for fire emissions. CAMS-GLOB-ANT v5.1  
162 provide monthly emissions and we generated daily files from the interpolation of the monthly  
163 values. The FINNv2.4 inventory provide daily fire emissions and are used directly. We update CO  
164 emission input files using the relative surface flux increments at every MOPITT CO assimilation  
165 step (6-hourly).

## 167 2.3 DART

168 DART is an open-source community facility for efficient ensemble data assimilation  
169 (<https://dart.ucar.edu/>). It is developed and maintained at the National Center for Atmospheric  
170 Research (NCAR). DART has been coupled with Community Atmosphere Model (CAM) for  
171 global meteorological data assimilation (CAM+DART; Raeder et al., 2012, 2021). Based on  
172 CAM+DART, the capability of chemical data assimilation using CAM-chem online chemistry and  
173 DART is developed and applied for scientific research (CAM-chem+DART; Arellano et al., 2007;  
174 Barré et al., 2015; Gaubert et al., 2016, 2017, 2020). Here, we use the Ensemble Adjustment  
175 Kalman Filter approach (EAKF; Anderson, 2001, 2003). The forecast ensemble is generated by  
176 30 CAM-chem simulations with different initial conditions and emissions. The assimilation is  
177 performed using DART and produces an ensemble of optimized initial conditions and emissions,  
178 as described in Gaubert et al. (2023). Specifically, the state vector includes CO initial conditions,  
179 and CO emission fluxes that are ascribed to fires and anthropogenic sources. We use ensemble

Deleted: 1

Deleted: priorvariance

Deleted: ;

Deleted: To assimilate meteorology and chemical observational data, an ensemble of 30 CAM-chem simulations with different initial conditions and emissions to generate the forecast ensemble at a given time. DART assimilates observations and produce the analysis, an ensemble of optimized initial conditions (see details in Gaubert et al., 2016).

190 mean at the forecast and the analysis step in the result sections. Ensemble mean of forecast is  
 191 denoted by

$$\bar{x}^f = \frac{1}{N} \sum_{j=1}^N x_j^f \quad (1)$$

192  
 193  
 194 ~~where~~  $\bar{x}^f$  is the ensemble mean of “forecast”, N is the ensemble size and  $x_j^f$  is the forecast value  
 195 of the j-th ensemble member. In our runs, DART uses ~~EAKF~~, a deterministic ensemble square root  
 196 filter for the analysis step. Unless noted otherwise, our setup is the same as in Gaubert et al., (2023).  
 197 We slightly change the emission update to include a correction to the previous day (t-1) in order  
 198 to smooth the emissions increments. Briefly, we apply multiplicative covariance inflation to the  
 199 forecast ensemble before each analysis step ~~to adjust the total error (model and observations) using~~  
 200 ~~the given observation error as reference (Anderson, 2007, 2009).~~ The inflation parameter is also  
 201 sequentially updated (Gharamti 2018) and varies in both space and time. ~~Localization is commonly~~  
 202 ~~used in ensemble-based data assimilation to address insufficient ensemble sample size.~~ ~~Since the~~  
 203 ~~correlation is expected to decrease as separation increases, it empirically reduces the impact of an~~  
 204 ~~observation on model state variable as a function of distance, using the Gaspari–Cohn localization~~  
 205 ~~function (Gaspari and Cohn, 1999).~~ The spatial localization horizontal half width is 600 km and  
 206 the vertical half width is 1200 m. The main difference between the profile and the column  
 207 assimilation resides in the vertical localization. ~~For each MOPITT retrieval, profile products have~~  
 208 ~~multiple observations at different layers but their impacts are vertically localized around 100 hPa.~~  
 209 ~~Therefore, not all vertical layers will be impacted. For the column data assimilation, there is no~~  
 210 ~~vertical localization in the column data assimilation except that the stratospheric (top 5) levels are~~  
 211 ~~not updated, as in the CO profile and meteorological DA.~~ ~~All vertical levels will be impacted by a~~  
 212 ~~single column value. In this case, if the mismatch is due to an underestimation of surface emissions~~  
 213 ~~rather than weak vertical transport, updating the upper tropospheric CO might lead to erroneous~~  
 214 ~~adjustments in CO abundance.~~

215  
 216 ~~Forward operators (denoted as H in DA terminology) are applied to project model field to~~  
 217 ~~observation space (i.e., expected observations). We use the forward operators introduced in Barré~~  
 218 ~~et al., (2015), consisting of i) estimating the log of a pressure weighted partial column volume~~  
 219 ~~mixing ratio that corresponds to the MOPITT grid and ii) applying the MOPITT averaging kernel~~  
 220 ~~and prior information as mentioned in section 2.1. In this study, we introduce an observation~~  
 221 ~~operator to assimilate the MOPITT columns in DART. That is, we estimate the retrieved column~~  
 222 ~~C (molecules cm<sup>-2</sup>), using the MOPITT prior column C<sub>a</sub> and following Equation 3 of the MOPITT~~  
 223 ~~Version 9 Product User's Guide:~~

$$C = C_a + a(x_{CAM-chem} - x_a) \quad (2)$$

224  
 225  
 226 ~~where~~  $x_{CAM-chem}$  and  $x_a$  are the modelled and the ~~MOPITT~~ a priori profiles expressed as  
 227 log<sub>10</sub>(VMR) and  $a$  is the total column averaging kernel. In this study, we assimilate both MOPITT  
 228 profile and column products and compare the results.

#### 230 2.4 Data assimilation experiments setup

231 There are 6 CAM-chem+DART runs (Figure 3). The first run is the spin-up/control run  
 232 that starts on July 1<sup>st</sup> 2018. The spin-up/control run only assimilates meteorological observations  
 233 and the state vector consists in wind, temperature, specific humidity, and surface pressure. Besides  
 234 the spin-up/control run, there are 5 experiment runs that assimilate different MOPITT CO  
 235 product(s) to update model CO. Note that the experiment runs not only assimilate MOPITT CO

- Deleted: Where where
- Deleted: the Ensemble Adjustment Kalman Filter (
- Deleted: ; Anderson et al., 2001, 2003)
- Deleted: to optimally adjust the ensemble spread to adjust the total error (model and observations) using the given observation error as reference (Anderson, 2007, 2009).
- Formatted: Font color: Text 1
- Deleted: Since the correlation is expected to decrease as separation increases, it
- Formatted: Font color: Text 1
- Deleted: using the Gaspari–Cohn localization function
- Formatted: Font color: Text 1
- Deleted: vertically
- Moved (insertion) [2]
- Deleted: T
- Formatted: Font color: Text 1
- Deleted: ¶
- Formatted: Font color: Text 1
- Deleted: mismatch due to rather than weak vertical transport updating CO lead to erroneous adjustments in CO abundance.
- Formatted: Font color: Text 1
- Moved up [2]: There is no vertical localization in the column data assimilation except that the stratospheric (top 5) levels are not updated, as in the CO profile and meteorological DA. ¶
- Deleted: as mentioned in section 2.1
- Deleted: In this case, the forward operators apply MOPITT averaging kernel and prior information to model CO field before comparing it to MOPITT products. The capability of assimilating MOPITT profile products is described in Barré et al., (2015).
- Deleted: an
- Deleted: in
- Deleted: That is, ¶
- Deleted: wWe
- Deleted: MOPITT
- Deleted: Where where
- Deleted: MOPITT
- Deleted: 2

269 products but also meteorological variables as in the spin-up/control run. The chemical state vector  
270 (CO and CO emissions) and the meteorological state vector do not impact each other. However,  
271 the updated meteorology due to meteorological data assimilation will impact the transport and  
272 possibly chemistry of CO during the forecast step. The 5 experiment runs are:

- 273 (1) Column JNT assimilation (Exp1-CJ);
- 274 (2) Profile JNT assimilation (Exp2-PJ);
- 275 (3) Column TIR assimilation (Exp3-CT);
- 276 (4) Column TIR and Column NIR assimilation (Exp4-CT+CN);
- 277 (5) Profile TIR and Column NIR assimilation (Exp5-PT+CN).

278 These 5 experiment runs are designed to address a few scientific questions:

- 279 • The comparisons of Exp1-CJ and Exp2-PJ will show the impacts of the assimilation of  
280 satellite profile versus column products.
- 281 • The comparisons of Exp1-CJ and Exp3-CT will show the difference caused by TIR-only  
282 product versus joint product.
- 283 • The comparisons of Exp1-CJ and Exp4-CT+CN will show the impacts of assimilating joint  
284 products (TIR+NIR) versus assimilating them separately for column products.
- 285 • The comparisons of Exp2-PJ and Exp5-PT+CN will show the impacts of assimilating joint  
286 products (TIR+NIR) versus assimilating them separately for profile products.

287 The experiment runs start on July 16<sup>th</sup> 2018 and are initialized with the spin-up/control run.

288 Each experiment runs for 35 days considering the cost and constrain of computational allocation.

289 The first 20 days (July 11<sup>th</sup> to July 15<sup>th</sup>, 2018) are CO spin-up and the last 15 days (July 31<sup>st</sup> to  
290 August 14<sup>th</sup>, 2018) are used for result analyses. The 15-day period are selected based on the spin-  
291 up time – as shown by fractions of observations rejected by the assimilation system (Figure 4).

292 Quality checks are common in data assimilation as the algorithms are employed operationally for  
293 near real time forecasting. We use the standard option in DART to do such quality checks. The  
294 absolute value of the difference between the observed value and the prior ensemble mean estimate  
295 is divided by the expected value of this difference. That expected value is the square root of the  
296 sum of the specified observation error variance and the prior ensemble variance. If this ratio is  
297 greater than a threshold, the observation is not used. The threshold ratio used here is three which  
298 is commonly used for large tropospheric applications in DART (e.g., Gaubert et al., 2023).  
299 Systematic errors are larger at the beginning of the spin-up, explaining the higher rejection rate.  
300 As the assimilation proceeds and the forecast bias is reduced, the rejection rate goes down. The  
301 experiments finished spinning up around 31 July. Each CAM-chem+DART run includes 30  
302 ensemble members. These 30 ensemble members have different initial conditions and emissions  
303 to represent model uncertainties. The analysis step is done every 6 hours. Anthropogenic and fire  
304 emissions are optimized separately on a daily basis following the method described in Gaubert et  
305 al. (2020, 2023).

## 306 2.5 CAM-chem simulations with updated emissions

307 To evaluate the updated emissions from the DA experiments, we conduct CAM-chem  
308 simulations for the same period using the ensemble mean of the updated fire and anthropogenic  
309 emissions. Hourly output is used for these simulations. Specifically, we conduct 6 CAM-chem  
310 simulations. Specifically, we conduct 6 CAM-chem  
311 simulations:

- 312 (S1) Simulation with emissions from Exp1-CJ;
- 313 (S2) Simulation with emissions from Exp2-PJ;
- 314 (S3) Simulation with emissions from Exp3-CT;

Deleted: changed updated

Formatted: Indent: First line: 0.5"

Deleted: (1) Column JNT assimilation; ¶

Deleted: (2) Profile JNT assimilation; ¶  
(3) Column TIR assimilation; ¶  
(4) Column TIR and column NIR assimilation; ¶  
(5) Profile TIR and column NIR assimilation. ¶

Deleted: experiment (1) and (2)

Deleted: experiment (1)

Deleted: (3)

Deleted: experiment (1)

Deleted: (4)

Deleted: experiment

Deleted: (2)

Deleted: (5)

Deleted: s

Deleted: 3

Deleted: ,

Deleted: t

Formatted: Font color: Black

Deleted: ¶

Deleted: (1) Column JNT assimilation

Deleted: (2) Profile JNT assimilation

Deleted: (3) Column TIR assimilation

337 (S4) Simulation with emissions from [Exp4-CT+CN](#);  
338 (S5) Simulation with emissions from [Exp5-PT+CN](#);  
339 (SControl) Simulation with original CAMS and FINN emissions.  
340

Deleted: (4) Column TIR and column NIR assimilation

Deleted: (5) Profile TIR and column NIR assimilation

### 341 3 Datasets used for results evaluation

#### 342 3.1 TROPospheric Monitoring Instrument (TROPOMI)

343 We use CO column retrieved from the TROPOMI instrument onboard the ESA's Sentinel-  
344 5 Precursor (Veeffkind et al., 2012) to evaluate model results. The spatial resolution of CO  
345 retrievals is  $\sim 5.5 \text{ km} \times 7 \text{ km}$  (Veeffkind et al., 2012; Borsdorff et al., 2018). TROPOMI CO data  
346 can be downloaded from <https://s5phub.copernicus.eu/dhus/#/home>. The TROPOMI Level 2 CO  
347 (Apituley et al., 2018) is used here. The TROPOMI data are filtered following Landgraf et al.  
348 (2018). To compare the model results with TROPOMI CO, we interpolate model outputs spatially  
349 and temporally to match the locations and times of TROPOMI CO retrievals, and then apply  
350 TROPOMI CO total column averaging kernels to the interpolated model CO profiles to obtain  
351 modeled total CO columns (Apituley et al., 2018). [TROPOMI CO data were compared to MOPITT](#)  
352 [CO in Martínez-Alonso et al., \(2020\). TROPOMI and MOPITT data show good agreement in](#)  
353 [terms of temporal and spatial patterns with global average biases <4% between all MOPITT CO](#)  
354 [column products \(TIR, NIR and JNT\) and TROPOMI. TROPOMI CO values were slightly lower](#)  
355 [than MOPITT in most regional comparisons.](#)  
356

#### 357 3.2 The Total Carbon Column Observing Network (TCCON)

358 TCCON is a network of ground-based Fourier Transform Spectrometers that records direct  
359 solar spectra in the NIR spectral region ([Wunch et al., 2011](#); [Laughner et al., 2023](#)). [TCCON data](#)  
360 [has been previously used to evaluate MOPITT products \(e.g., Hedelius, et al., 2019\).](#) Column-  
361 averaged mixing ratios of chemical species such as  $\text{CO}_2$ ,  $\text{CH}_4$ ,  $\text{N}_2\text{O}$ , and CO are retrieved from  
362 these spectra. We use CO column data from the TCCON GGG2020 data release  
363 (<https://tccodata.org/2020>; TCCON Team, 2022) to evaluate model results. [Data from 18](#)  
364 [TCCON sites are used \(Buschmann et al., 2022; García et al., 2022; Hase et al., 2022; Iraci et al.,](#)  
365 [2022; Kivi et al., 2022; Liu et al., 2022; Morino et al., 2022a, 2022b, 2022c; Notholt et al., 2022;](#)  
366 [Pollard et al., 2022; Shiomi et al., 2022; Té et al., 2022; Warneke et al., 2022; Wennberg et al.,](#)  
367 [2022a, 2022b; Wunch et al., 2022\).](#) We interpolate model results to TCCON data locations and  
368 time and apply TCCON averaging kernels to model results for proper comparisons.  
369

Deleted: ¶

#### 370 3.3 NOAA Carbon Cycle Greenhouse Gases (CCGG) sites

371 We use the atmospheric CO dry air mole fractions from the NOAA GML Carbon Cycle  
372 Cooperative Global Air Sampling Network  
373 ([https://gml.noaa.gov/aftp/data/trace\\_gases/co/flask/surface/](https://gml.noaa.gov/aftp/data/trace_gases/co/flask/surface/); Petron et al., 2022). Event data are  
374 used. The reference scale is WMO CO\_X2014A. We interpolate model results to CCGG site  
375 locations and time for proper comparisons. Note that on average, each site only has data on  $\sim 4$   
376 days and  $\sim 9$  data points in total from July 16th, 2018 to August 14th, 2018.  
377

#### 378 3.4 In-service Aircraft for a Global Observing System (IAGOS)

379 IAGOS is a European research infrastructure developed for operations on commercial  
380 aircraft to monitor atmospheric composition (Petzold et al., 2015). The IAGOS instrument package  
381 1 measures CO as well as  $\text{O}_3$ , air temperature, and water vapor (<https://www.iagos.org/iagos-core->  
382

386 instruments/package1/). CO is measured by infrared absorption using the gas filter correlation  
387 technique (Precision:  $\pm 5\%$ , Accuracy:  $\pm 5$  ppb). Here we use vertical profiles of CO from IAGOS  
388 for model evaluation. We use CO profiles in North and West Africa, Tropical Asia, East Asia,  
389 Europe, Eastern North America, Western North America, Central and South America, and Middle  
390 East and conduct evaluation in these regions separately. CO profiles used and regions is shown in  
391 Figure S2. Note that IAGOS profiles are divided into regions based on their locations, however  
392 the IAGOS profiles in a region are not representative of the whole region due to coverage (Figure  
393 S2).  
394

### 395 **3.5 Western wildfire Experiment for Cloud chemistry, Aerosol absorption and Nitrogen** 396 **(WE-CAN)**

397 The WE-CAN field campaign was conducted over the Northwestern U.S. during July–  
398 September 2018 (<https://data.eol.ucar.edu/project/WE-CAN>). There were 16 research flights of  
399 the NCAR/NSF C-130 research aircraft during the campaign. Our experiment runs start on July  
400 16<sup>th</sup> and end on August 14<sup>th</sup>. Therefore, we compare the model results to measurements from  
401 flights on July-31, August-02, August-03, August-06, August-08, August-09, and August-13. We  
402 use 1-minute averaged CO (Picarro G2401-mc) data. Model results are interpolated to match  
403 locations and time of the observations, and then both interpolated model results and observations  
404 are averaged back to the model spatial resolution ( $1.25^\circ$  in longitude and  $0.95^\circ$  in latitude), 6-  
405 hourly bins, and 50 hPa vertical layers. This is because the model spatial and temporal resolution  
406 are much lower than observations and model results cannot reproduce the high variability in the  
407 raw observations.  
408

## 409 **4. Diagnostics of the assimilation results**

### 410 **4.1 Observation space diagnostics**

#### 411 **4.1.1 Fractions of observations rejected by the assimilation system**

412 In all the five experiments, the assimilation improves the agreement between model  
413 forecast and observations of not only the MOPITT products assimilated but also the MOPITT  
414 products that were not assimilated. Assimilating MOPITT CO column product(s) improves model  
415 agreement with MOPITT CO profile product(s) and vice versa. Figure 4 shows time series of the  
416 fraction of observations rejected by the assimilation system (%) when they are too far from the  
417 model ensemble mean. The decreasing fractions with time indicate more observations being  
418 accepted by the model, i.e., and observations and modeled values are getting closer in later time  
419 steps. For a MOPITT product that is not assimilated in an experiment run, it is still used in the  
420 “evaluation mode”, where the ensemble is run through the observation operator, but not  
421 assimilated. Therefore, the hypothetical fraction of observations rejected is still calculated for the  
422 MOPITT product for that experiment run, even though these observations are not assimilated. For  
423 the spin-up/control run, there is no significant trend for the fractions of rejected observations  
424 (Figure 4f). For the five experiments, the fractions of rejected observations decrease with time.  
425 Assimilating (Figures 4a–4e) any MOPITT product(s) improves model agreement with all the five  
426 MOPITT CO products regardless if they are column or profile products. When only assimilating  
427 column products (Exp1-CJ; Exp3-CT; and Exp4-CT+CN), the fraction of rejected observations  
428 decreases faster than that when assimilating both profile and column products (Exp5-PT+CN). For  
429 experiments that assimilate profiles (Exp2-PJ and Exp5-PT+CN), the fractions of rejected  
430 observations decrease slower than the other three experiments that only assimilate column

Deleted: Results

Deleted: 3

Deleted: 3

Deleted: 3

Deleted: 3

Deleted: (1) Column JNT assimilation

Deleted: (3) Column TIR assimilation

Deleted: (4) Column TIR and column NIR assimilation

Deleted: (5) Profile TIR and column NIR assimilation

Deleted: Experiments (2) and (5)



441 products ([Exp1-CJ](#), [Exp3-CT](#), and [Exp4-CT+CN](#)). This is expected because profile assimilation  
 442 has relatively small impact than column assimilation overall due to vertical localization.

#### 444 4.1.2 Reduced centered random variable (RCRV) and chi-square statistics $\chi^2$

445 We use the RCRV as a diagnostic of the ensemble bias (Candille et al., 2007) and has been  
 446 previously used to validate assimilation results (e.g., Gaubert et al., 2014). Mean RCRV for P  
 447 observations is defined by the ratio between the innovation and its associated error:

$$448 \quad RCRV = \frac{1}{P} \sum_{i=1}^P \frac{y_i^o - Hx_i^f}{\sqrt{\sigma_{o,i}^2 + \sigma_{f,i}^2}} \quad (3)$$

449 Where  $y_i^o$  is the value of i-th observation,  $Hx_i^f$  gives the expected observation from the model,  $\sigma_{o,i}^2$   
 450 is the observation error variance, and  $\sigma_{f,i}^2$  is the ensemble variance. The mean of the RCRV  
 451 represents the weighted bias of the forecast, and hence a value close to 0 indicates the ensemble is  
 452 representative (i.e., error variances are comparable to the innovations). Figure 5 shows daily  
 453  $RCRV$ . For a given experiment, only  $RCRV$  of MOPITT product(s) assimilated in the experiment  
 454 is shown here. In most cases  $RCRV$  is close to zero, indicating that the ensemble is representative.  
 455 The only exceptions are NIR column product in [Exp4-CT+CN](#) and [Exp5-PT+CN](#).

456 Chi-square statistics ( $\chi^2$ ) is also used to verify an effective assimilation by comparing error  
 457 specifications and their balance with actual model-observation mismatch (Ménard and Chang,  
 458 2000) and has been previously used to evaluate assimilation results (e.g., Gaubert et al., 2016;  
 459 Sekiya et al., 2021). Mean RCRV for P observations is defined as

$$460 \quad \bar{\chi}^2 = \frac{1}{P} \sum_{i=1}^P \frac{(y_i^o - Hx_i^f)^2}{\sigma_{o,i}^2 + \sigma_{f,i}^2} \quad (4)$$

461 A value lower than 1 indicates an overfitting of the observations while a value higher than 1  
 462 suggests an underestimation of the actual model and observation mismatch. Daily  $\bar{\chi}^2$  are also  
 463 shown in Figure 5. The  $\bar{\chi}^2$  values are all higher than 1 indicating an underestimation of the actual  
 464 model and observation mismatch. However,  $\bar{\chi}^2$  decreases with time and gradually approaches  
 465 towards 1, indicating the degree of such underestimation decreases with time.

#### 467 4.2 Model space diagnostics

468 We analyze the impacts of assimilating MOPITT CO products by comparing the  
 469 experiment runs with control/spin-up run, which effectively isolate the signal resulting from the  
 470 CO assimilation. Figure 6 show the spatial distribution of CO difference caused by assimilation  
 471 (CO from forecast of experiment minus CO from the control/spin-up run) for the 5 experiments  
 472 (15-day average). At the surface, the spatial distributions of CO difference are similar among the  
 473 5 experiments. In line with Gaubert et al. (2023), the 5 experiments show overall higher CO in the  
 474 Northern Hemisphere and lower CO in the tropics and India compared to the control/spin-up run.  
 475 [Exp2-PJ](#) and [Exp5-PT+CN](#) reduce CO in California which is not the case for other experiments.  
 476 [Exp2-PJ](#) and [Exp5-PT+CN](#) are the only two experiments that involves profile product assimilation.  
 477 In addition, profile JNT is retrieved with profile TIR and column NIR therefore [Exp2-PJ](#) is  
 478 expected to assimilate similar information as [Exp5-PT+CN](#). In addition, when comparing [Exp1-](#)  
 479 [CJ](#) and [Exp1-PJ](#), column assimilation has a larger downwind impact (e.g., the ocean between  
 480 Africa and South America). At 500 hPa, the 5 experiments still show overall higher CO in the  
 481 Northern Hemisphere compared to the control/spin-up run. However, the [Exp2-PJ](#) and (5) that  
 482 involve profile assimilation have lower CO values than the other 3 experiments, especially in the  
 483 high latitudes. At 200 hPa, the spatial distribution of the CO difference caused by assimilation is

Deleted: Experiments (1), (3), and (4)

Deleted: 4

Deleted: (4) Column TIR and column NIR assimilation

Deleted: (5) Profile TIR and column NIR assimilation

Deleted: 4

Deleted: 5

Deleted: ,

Deleted: Experiment (2) Profile JNT assimilation

Deleted: Experiment (5) Profile TIR and column NIR  
assimilation...

Deleted: Experiment (2) Profile JNT assimilation

Deleted: Experiment (5) Profile TIR and column NIR  
assimilation...

Deleted: Experiment (2) Profile JNT assimilation

Deleted: (5) Profile TIR and column NIR assimilation

Deleted: Experiments (1) and (2)

Deleted: Experiment (2)

Deleted: include

502 smallest in Exp2-PJ, followed by Exp5-PT+CN. On the contrary, for the other three experiments  
503 which do not involve profile assimilations, the spatial distribution of the CO difference caused by  
504 assimilation is relatively large, i.e., assimilating MOPITT profile product(s) only slightly changes  
505 CO values at 200 hPa whereas assimilating MOPITT column product(s) changes CO values at 200  
506 hPa dramatically. This is expected as vertical distribution is often an advantage of profile DA that  
507 column DA cannot represent.

508 Assimilating profile products have different vertical impacts from assimilating column  
509 products (Figure 7). Overall, the two experiments that involve profile assimilation (Exp2-PJ and  
510 Exp5-PT+CN) seem to be close to each other, while the other three experiments that only involve  
511 column assimilation (Exp1-CJ, Exp3-CT, and Exp4-CT+CN) also exhibit similarities among  
512 themselves. Globally speaking, experiments that assimilate only column product(s) have a larger  
513 impact at and near the surface compared to experiments that assimilate only profile product(s)  
514 (Figures 7a and 7b). This is reasonable because profile assimilation is more localized vertically.  
515 Regional speaking, the impacts of the five experiments vary across continents.

516 The difference caused by assimilating profile products is in general smaller than the  
517 difference caused by assimilating column products. The exceptions are Africa and South America  
518 where the two experiments that assimilate profiles have lower CO than the three experiments that  
519 only assimilate columns between 900 hPa and 600 hPa. CO over the two regions is dominated by  
520 fire emissions during the experiment period. It is known that FINN overestimates fire emissions  
521 in the tropics (Wiedinmyer et al., 2023; Gaubert et al., 2023) of CO which were transported to  
522 upper levels through fire plume rise and tropical convection. This overestimation between 900 hPa  
523 and 600 hPa is corrected by assimilating MOPITT CO products, especially profile products that  
524 captured CO plumes between 900 hPa and 600 hPa. Exp2-PJ and Exp5-PT+CN have some  
525 relatively small differences over some regions even though profile JNT is retrieved with profile  
526 TIR and column NIR. For example, over North America, Exp2-PJ has lower CO values than Exp5-  
527 PT+CN. Exp1-CJ and Exp4-CT+CN are in general similar with some exceptions. For example,  
528 over Africa between 900 hPa and 600 hPa, CO profile from Exp1-CJ is closer to Exp3-CT rather  
529 than Exp4-CT+CN.

## 531 5 Comparisons with independent observations

### 532 5.1 TROPOMI

533 To evaluate the results, we compare the CO from DA forecasts with independent  
534 observations. Comparisons with TROPOMI CO column retrievals are shown in Figure 8. The  
535 control run underestimates background CO in the Northern Hemisphere while overestimates CO  
536 near fire source regions in the tropics and Southern Hemisphere. Compared to the control run, all  
537 five of the experiments show improved agreement with TROPOMI CO by increasing background  
538 CO in the Northern Hemisphere and reducing CO near fire source regions in the tropics and  
539 Southern Hemisphere. The spatial distributions of the mean biases from the three experiments with  
540 only column assimilation are close while those from the two experiments with profile assimilation  
541 are close. The two experiments with profile assimilations have smaller improvement for  
542 background CO in the Northern Hemisphere. This is reasonable because profile assimilation has  
543 relatively small impact than column assimilation due to tight vertical localization. However, near  
544 the fire source regions, the two experiments with profile assimilations have lower biases than the  
545 three experiments with only column assimilation. This is the case not only in Africa, South  
546 America and tropical Asia (Figure 8), but also in California (fire region) and Nevada (downwind  
547 of the fire region), USA during the study period which is the fire season in the region (Figure S5).

Deleted: ,i

Deleted: 6

Deleted: Experiments (2) and (5)

Deleted: Experiments (1), (3), and (4)

Deleted: 6

Deleted: 6

Deleted: Experiment (2) Profile JNT assimilation

Deleted: Experiment (5) Profile TIR and column NIR  
assimilation...

Deleted: (2) Profile JNT assimilation

Deleted: Experiment (5) Profile TIR and column NIR  
assimilation...

Deleted: Experiment (1) Column JNT assimilation

Deleted: Experiment (4) Column TIR and column NIR  
assimilation...

Deleted: Experiment (1) Column JNT assimilation

Deleted: Experiment (3) Column TIR assimilation

Deleted: Experiment (4) Column TIR and column NIR  
assimilation...

Deleted: 7

Deleted: 7

569 This indicates profile assimilation can out-perform column assimilations in circumstances with  
570 fire impacts, which is likely due to transport errors and fire plume rise that requires vertical  
571 information to resolve plume locations.

## 572 5.2 TCCON

573 Overall, the control run tends to underestimate CO and the 5 experiments all agree better  
574 with TCCON observations compared to the control run but still underestimates CO in general  
575 (Figure 9). Column assimilations (Exp1-CJ, Exp3-CT, and Exp4-CT+CN) significantly  
576 overestimate CO at pasadena01 and edwards01 sites in California, USA during 26 July 2018 to 04  
577 August 2018, likely due to fire impacts. The significant overestimation is not seen in the two  
578 experiments with profile assimilations (Exp2-PJ and Exp5-PT+CN). This is consistent with the  
579 comparison results with TROPOMI and implies the profile assimilation can out-perform column  
580 assimilations in fire-impacted regions. The model-observation discrepancies overall decrease with  
581 time. A time series of TCCON and modeled CO columns is shown in Figure S6.

## 582 5.3 CCGG sites

583 All experiments show improved agreement with surface in-situ CO observations from  
584 CCGG sites compared to the control run (Figure 10), as shown by with higher correlations (0.6-  
585 0.65 versus 0.56) and lower model biases (0.7-4.91 ppb versus 8.6 ppb). As for RMSE, however,  
586 the experiments do not reduce RMSE compared to the control run (34-50 ppb versus 36 ppb).  
587 Exp1-CJ has the lowest mean bias (5.7 ppb) while Exp5-PT+CN have the highest correlation  
588 (0.79).

589 Spatial distributions of model bias in CO (ppb) against CO observations from CCGG sites  
590 are shown in Figures S7-S10. The UTA CCGG site is close to the two TCCON sites in California,  
591 USA (pasadena01 and edwards01). All the five experiments significantly underestimate CO at the  
592 UTA surface site during 26 July 2018 to 4 August 2018, whereas the five experiments overestimate  
593 CO compared to the two TCCON sites (Figure 9). This inconsistency is likely due to (1) UTA  
594 CCGG site measures CO at the surface while the TCCON sites measure column total CO; (2) there  
595 are only two data points during that period at the UTA site and are not comparable to the sampling  
596 of the two TCCON sites.

## 597 5.4 IAGOS

598 Globally, all five experiments agree better with IAGOS CO profiles compared to the  
599 control run (Figure 11a). At the 900-1000 hPa layer, Exp2-PJ has the lowest bias, followed by  
600 Exp4-CT+CN. At layers above 800 hPa, the three experiments with only column assimilation have  
601 lower bias. CO bias of Exp1-CJ and Exp4-CT+CN are very similar using that of Exp3-CT as a  
602 reference. This is expected as Column JNT product contains similar information as column TIR  
603 product and column NIR products together. Above 200 hPa, all five experiments overall agree  
604 better with IAGOS CO compared to the control run. However, experiments involving profile  
605 assimilation do not show obvious differences compared to experiments only involving column  
606 assimilation above 200 hPa. Over most regions, the five experiments show improved agreement  
607 with IAGOS data except for Tropical Asia and Central and South America where the five  
608 experiments have similar or larger biases (Figure 11). Over North and West Africa, the control run  
609 has positive bias whereas the five experiments have negative biases below 500 hPa, indicating the  
610 system might over-adjust in the region. The comparisons with IAGOS show that the experiments  
611 overall perform better in the Northern Hemisphere than in the tropics.

Deleted: 8

Deleted: Experiments (1), (3), and (4)

Deleted: Experiments (2) and (5)

Deleted: 9

Deleted: Experiment (1) Column JNT assimilation

Deleted: 0.7

Deleted: Experiment (2)

Deleted: Profile JNT assimilation

Deleted: 65

Deleted: (1) Column JNT assimilation, (2) Profile JNT assimilation, (3) Column TIR assimilation, (4) Column TIR and column NIR assimilation, and (5) Profile TIR and column NIR assimilation.

Deleted: 8

Deleted: 0

Deleted: Experiment (2) Profile JNT assimilation

Deleted: Experiment (4) Column TIR and column NIR assimilation...

Deleted: Experiments (1) Column JNT assimilation

Deleted: (4) Column TIR and column NIR assimilation

Deleted: (3) Column TIR assimilation

Deleted: 0

637  
638  
639  
640  
641  
642  
643  
644  
645  
646  
647  
648  
649  
650  
651  
652  
653  
654  
655  
656  
657  
658  
659  
660  
661  
662  
663  
664  
665  
666  
667  
668  
669  
670  
671  
672  
673  
674  
675  
676  
677  
678  
679  
680  
681  
682

## 5.5 WE-CAN

The experiments do not show improvement from the control run when compared to airborne measurements from WE-CAN. This is expected because the airborne measurements during WE-CAN aimed to sample fire plumes and include extremely high CO concentrations which are challenging for a 1-degree global model to capture, not to mention the output is 6-hourly. The experiments only do show lower model bias than the control run (-24 to -48 ppb versus -52 ppb), however the difference between [Exp2-PJ](#) and [Exp5-PT+CN](#) from the control run is small. The correlation and RMSE of the experiments are not improved. The subtle improvement in the mean bias is likely driven by large-scale adjustment rather than improvement in resolving flight-scale features.

## 6. Emissions

### 6.1 Emission updates

Assimilating profile products ([Exp2-PJ](#) and [Exp5-PT+CN](#)) tends to have a larger change to the emissions compared to only assimilating column products ([Exp1-CJ](#), [Exp3-CT](#), and [Exp4-CT+CN](#)). [As shown previously, profile assimilation can out-perform column assimilations near the surface due to vertical localization. Different CO concentrations at and near the surface resulted in different emission updates between profile assimilation and column assimilation.](#) The 5 experiments overall increase anthropogenic CO emissions while reduce fire CO emissions ([Figure 13](#)). For anthropogenic emissions, the two experiments that assimilate CO profiles ([Exp2-PJ](#) and [Exp5-PT+CN](#)) significantly increase anthropogenic CO emissions from ~500 Tg/year to ~700 Tg/year globally in August, which is not the case for the other experiments. Anthropogenic emissions in India are reduced by the experiments while in East Asia are increased ([Figure 14](#)). Fire emissions are reduced by the 5 experiments in Africa and South America and the reduction is the largest for the two experiments that assimilate CO profiles ([Figures 13](#), and [14](#)). This is consistent with the conclusion in [Wiedinmyer et al. \(2023\)](#), which found fire emissions in FINNv2.4 over Africa are too high, and consequently were reduced in FINNv2.5. The experiments overall increase fire emissions in North America, indicating that FINNv2.4 underestimates fire emissions in the region during the assimilation period. Fire and anthropogenic emissions can have different injection heights and impact different vertical levels. This is especially the case for regions with strong convection (e.g., central Africa).

### 6.2 CAM-chem simulations with updated emissions

We compared the CAM-chem simulations with updated emissions and original emissions to CO observations from TROPOMI, TCCON, CCGG site, IAGOS, and WE-CAN ([Figures S11-S18](#)). The five simulations with updated emissions overall show better agreement with observations compared to the control run with original emissions. Simulations using emissions from profile assimilation experiments (Simulations (S2) and (S5)) in general perform better than column assimilation especially near the surface (S17) and at fire source regions ([Figures S11, S12, and S14](#)). This is consistent with the evaluation of DA experiments. This indicates assimilating satellite profiles can perform better near the surface and have a larger impact on emissions compared to only assimilating column products.

## 7. Discussions

### 7.1 Assimilating multispectral product versus TIR-only product

Deleted: Experiments (2)

Deleted: (5)

Deleted: Experiments (2) and (5)

Deleted: Experiments (1), (3), and (4)

Deleted: Experiments (2) and (5)

Deleted: 3

Deleted: 2

Deleted: 3

691 The comparisons between [Exp1-CJ](#) and [Exp3-CT](#) demonstrate the impacts of assimilating  
692 satellite multispectral/joint products versus TIR-only products. Overall, when comparing to  
693 independent CO column observations, assimilating joint products do not show clear improvement  
694 from assimilating TIR-only products (Figures [8](#) and [9](#)). However, when comparing to independent  
695 CO profile observations or surface CO observations, assimilating joint products leads to better  
696 model-observation agreement at and near the surface (Figures [10](#) and [11](#)). This is reasonable as  
697 the joint MOPITT product has enhanced sensitivity to near-surface CO (Worden et al., 2010).

## 7.2 Assimilating profile product versus column product

700 The comparisons between [Exp1-CJ](#) and [Exp2-PJ](#) demonstrate the impacts of assimilating  
701 satellite multispectral/joint products versus TIR-only products. The fractions of rejected  
702 observations for [Exp3-CT](#) decrease slower than [Exp1-CJ](#) due to vertical localization when  
703 assimilating profile products. For the same reason, assimilating column products has a larger  
704 impact on the analysis compared to assimilating profile products. Therefore, [Exp2-PJ](#) with profile  
705 assimilation has smaller improvement for background and large-scale CO in the northern  
706 hemisphere (Figure [8](#)) compared to [Exp1-CJ](#) with column assimilation. However, assimilating  
707 profile products can have different vertical impacts from assimilating column products (figure [7](#)).  
708 Profile assimilation can out-perform column assimilations in fire-impacted regions and near the  
709 surface (Figure [11](#)).

710 Assimilating profile products tends to have a larger change to the emissions compared to  
711 only assimilating column products. Simulations using emissions from profile assimilation  
712 experiments in general perform better than column assimilation especially near the surface and at  
713 fire source regions.

## 7.3 Assimilating multispectral product versus assimilating TIR and NIR separately

716 For multispectral/joint products, we also compare the impacts of assimilating the joint  
717 product directly versus assimilating the single spectral products separately. MOPITT column JNT  
718 products are retrieved from MOPITT column TIR and column NIR products, while MOPITT  
719 profile JNT products are retrieved from MOPITT profile TIR and NIR products. Therefore, we  
720 compare [Exp1-CJ](#) to [Exp4-CT+CN](#), [Exp2-PJ](#) to [Exp5-PT+CN](#) for demonstration. In general,  
721 assimilating multispectral/joint products result in similar or slight better agreement with  
722 observations compared to assimilating the single-spectral products separately. This is the case for  
723 both assimilating profile products ([Exp2-PJ](#) versus [Exp5-PT+CN](#)) and column products ([Exp1-CJ](#)  
724 versus [Exp4-CT+CN](#)). In addition, assimilating multispectral/joint products is more  
725 computationally efficient than assimilating single spectral products separately. These two reasons  
726 point to the benefit of developing multispectral/joint products for CO as well as other species such  
727 as O<sub>3</sub> and CH<sub>4</sub> and assimilating them in DA systems.

## 7.4 Limitation

730 Here we only conduct experiments for 15 days [as the number of experiments and](#)  
731 [computational cost prohibit longer simulations. A previous study performed longer simulations for](#)  
732 [one experiment that assimilated the MOPITT profile product for a whole year \(Gaubert et al.,](#)  
733 [2016\) and found that there is no significant seasonal change in the performance of the CAM-](#)  
734 [chem+DART. If observations of roughly the same quality/quantity are available in other years, the](#)  
735 [performance of the DA might be expected to be similar. However, more research is needed to fully](#)  
736 understand the impact of (1) assimilating multispectral/joint products versus single-spectral

Deleted: experiment (1) Column JNT assimilation

Deleted: (3) Column TIR assimilation

Deleted: 7

Deleted: 8

Deleted: 9

Deleted: 0

Deleted: experiment (1) Column JNT assimilation

Deleted: (2) Profile JNT assimilation

Deleted: Experiment (3)

Deleted: experiment (1)

Deleted: experiment (2)

Deleted: 7

Deleted: experiment (1)

Deleted: 6

Deleted: 0

Deleted: Experiment (1)

Deleted: Experiment (4)

Deleted: Experiment (2)

Deleted: Experiment (5)

Deleted: Experiments (2)

Deleted: (5)

Deleted: Experiments (1)

Deleted: (4)

Deleted: due to limitation in computational resources. The 15 days in July and August 2018 may not be representative of other seasons and years.

Deleted: M

764 products, (2) the comparison of satellite profiles and satellite columns DA, and (3) assimilating  
 765 multispectral or each product separately. This study provides guidance for future work on the  
 766 assimilation of multi-spectral satellite retrievals of atmospheric composition using MOPITT as a  
 767 demonstration. However, whether the conclusions based on MOPITT CO are applicable to other  
 768 species (e.g., CH4 and O3) needs further study. Nevertheless, the results and conclusions presented  
 769 in this study are valid and shed light on the impacts of assimilating different satellite products of  
 770 the same atmospheric composition.

771 The CAM-chem+DART experiments in this study overall show improvement in  
 772 background and large-scale CO distributions compared to the control/spin-up run, as shown by the  
 773 comparisons with global observations such as TROPOMI and TCCON. However, CAM-  
 774 chem+DART improvement on small-scale features is challenging due to limitation in model  
 775 resolution, as shown by the comparisons with airborne measurements during WE-CAN. A higher  
 776 resolution DA system is needed to resolve these features. We are currently developing the  
 777 capability of DA using MUSICA+DART which will address this issue (Pfister et al., 2020).  
 778 MUSICA has already been shown to better resolve fires at higher resolution while still addressing  
 779 global-scale impacts (Tang et al., 2022, 2023).

## 781 8. Conclusions

782 We conduct 6 CAM-chem+DART assimilation runs for 15 days (July 31st, 2018 to August  
 783 14<sup>th</sup>, 2018) to understand the impact of (1) assimilating multispectral products versus single-  
 784 spectral products, (2) assimilating satellite profile products versus column products, and (3)  
 785 assimilating multispectral products versus assimilating individual products separately. The DA  
 786 runs include 1 control run that only assimilates meteorological variables and 5 experiment runs  
 787 that assimilate meteorological variables and different MOPITT product(s), namely Exp1-  
 788 CJ; Exp2-PJ; Exp3-CT; Exp4-CT+CN; and Exp5-PT+CN. We then compare the results with  
 789 independent CO observations from satellite, ground-based remote sensing, surface and aircraft  
 790 observations (TROPOMI, TCCON, CCGG sites, IAGOS, and WE-CAN). Fire and anthropogenic  
 791 emissions of CO are also optimized in the DA experiments. We conduct 5 CAM-chem runs with  
 792 the 5 sets of optimized emissions to understand the impacts of assimilating different MOPITT  
 793 products. We also conduct 1 additional CAM-chem runs with original emissions for reference. The  
 794 main findings are as follows:

795 (1) Assimilating MOPITT profile products improves model agreement with MOPITT  
 796 column products and vice versa.

797 (2) All five DA experiments show improved agreement with CO observations from  
 798 TROPOMI, TCCON, CCGG sites, and IAGOS compared to the control/spin-up run. Assimilating  
 799 MOPITT joint column product leads to better model-observation agreement at and near the surface  
 800 than assimilating MOPITT TIR-only column product.

801 (3) Assimilating profile products tends to have a larger change to the emissions compared  
 802 to only assimilating column products. The five experiments overall increase anthropogenic CO  
 803 emissions while reducing fire CO emissions. The five CAM-chem simulations with updated  
 804 emissions overall show better agreement with observations compared to the control run with  
 805 original emissions. Simulations using emissions from profile assimilation experiments in general  
 806 perform better than column assimilation especially near the surface and at fire source regions.

807 (4) Assimilating column products has larger impacts and improvement for background and  
 808 large-scale CO compared to assimilating profile products due to vertical localization in profile

**Deleted:** (1) Column JNT assimilation

**Deleted:** (2) Profile JNT assimilation

**Deleted:** (3) Column TIR assimilation

**Deleted:** (4) Column TIR and column NIR assimilation

**Deleted:** (5) Profile TIR and column NIR assimilation

**Deleted:** (2) The five experiments show overall higher CO in the Northern Hemisphere and lower CO in the tropics and India compared to the control/spin-up run.¶

**Deleted:** 3

**Moved (insertion) [1]**

**Deleted:** (6)

**Deleted:** ¶

Results were not improved compared to WE-CAN because .....

**Deleted:** 4

**Deleted:** ¶

(5)

**Moved up [1]:** (6) Assimilating MOPITT joint column product leads to better model-observation agreement at and near the surface than assimilating MOPITT TIR-only column product.¶

**Deleted:** 7

830 assimilation. However, profile assimilation can out-perform column assimilations in fire-impacted  
831 regions and near the surface.

832 (5) Assimilating multispectral/joint products result in similar or slightly better agreement  
833 with observations compared to assimilating the single-spectral products separately. Assimilating  
834 multispectral/joint products is also more computationally efficient than assimilating single spectral  
835 products separately. Therefore, it is advantageous to develop multispectral/joint products for CO  
836 as well as other species (e.g., O<sub>3</sub> and CH<sub>4</sub>) and assimilating them in DA systems.

837  
838

### 839 Competing interests

840 At least one of the (co-)authors is a member of the editorial board of Atmospheric Measurement  
841 Techniques.

842

### 843 Acknowledgement

844 This project is partially supported by NOAA Atmospheric Chemistry, Carbon Cycle and Climate  
845 (AC4) Program (Award Number: NA22OAR4310204). This material is based upon work  
846 supported by the National Center for Atmospheric Research, which is a major facility sponsored  
847 by the National Science Foundation under Cooperative Agreement No. 1852977. We would like  
848 to acknowledge high-performance computing support from Cheyenne (doi:10.5065/D6RX99HX)  
849 provided by NSF NCAR's Computational and Information Systems Laboratory, sponsored by the  
850 National Science Foundation. We thank TROPOMI, TCCON, NOAA CCGG, IAGOS, and WE-  
851 CAN team for observational data. The TCCON data were obtained from the TCCON Data Archive  
852 hosted by CaltechDATA at <https://tccondata.org>.

853

### 854 Author contribution

855 Conceptualization, HMW; Investigation, WT and BG; Methodology, BG, WT, HMW, and LKE;  
856 Formal analysis, WT and BG; Data curation, DZ, DM, KR, and JLA; Validation, WT;  
857 Visualization, WT; Supervision, HMW; Writing – original draft preparation, WT, BG, and HMW;  
858 Writing – review & editing, LKE, DPE, AFA, DZ, DM, KR, and JLA.

859

### 860 References

861 Anderson, J.L. An ensemble adjustment Kalman filter for data assimilation. *Monthly weather*  
862 *review*, 129(12), pp.2884-2903, 2001.

863

864 Anderson, J.L. A local least squares framework for ensemble filtering. *Monthly Weather Review*,  
865 131(4), pp.634-642, 2003.

866

867 Anderson, J.L. An adaptive covariance inflation error correction algorithm for ensemble filters.  
868 *Tellus A: Dynamic meteorology and oceanography*, 59(2), pp.210-224, 2007.

869

870 Anderson, J. Spatially and temporally varying adaptive covariance inflation for ensemble filters.  
871 *Tellus A: Dynamic meteorology and oceanography*, 61(1), pp.72-83, 2009.

872

873 Anderson, J. L., T. Hoar, K. Raeder, H. Liu, N. Collins, R. Torn and A. Arellano: The Data  
874 Assimilation Research Testbed: A Community Facility. *Bulletin of the American Meteorological*  
875 *Society*, 90, 1283-1296, doi:10.1175/2009BAMS2618.1, 2009.

Deleted: 8

Deleted: (9) CAM-chem+DART improvement on small-scale features is challenging due to limitation in model resolution. We are currently developing the capability of DA using MUSICA+DART (a higher resolution DA system) to address this issue.

Deleted: , 2001

Deleted: , 2003.

884  
885  
886 Apituley, A., Pedergrana, M., Sneep, M., Pepijn Veeffkind, J., Loyola, D., Landgraf, J., Borsdorff,  
887 T., 2018. Sentinel-5 Precursor/TROPOMI Level 2 Product User Manual Carbon Monoxide,  
888 SRON-S5P-LEV2-MA-002. Royal Netherlands Meteorological Institute.  
889  
890 Arellano Jr, A.F., Raeder, K., Anderson, J.L., Hess, P.G., Emmons, L.K., Edwards, D.P., Pfister,  
891 G.G., Campos, T.L. and Sachse, G.W., 2007. Evaluating model performance of an ensemble-based  
892 chemical data assimilation system during INTEX-B field mission. *Atmospheric Chemistry and*  
893 *Physics*, 7(21), pp.5695-5710.  
894  
895 Barré, J., B. Gaubert, A. F. J. Arellano, H. M. Worden, D. P. Edwards, M. Deeter, J. L. Anderson,  
896 K. D. Raeder, N. S. Collins, S. Tilmes, G. Francis, C. Clerbaux, L. Emmons, G. Pfister, P.-F.  
897 Coheur and D. Hurtmans, 2015. Assessing the impacts of assimilating IASI and MOPITT CO  
898 retrievals using CESM-CAM-chem and DART. *Journal of Geophysical Research: Atmospheres*,  
899 120, no. 19, doi:10.1002/2015JD023467  
900  
901 Borsdorff, T., Aan de Brugh, J., Hu, H., Aben, I., Hasekamp, O., & Landgraf, J. (2018). Measuring  
902 carbon monoxide with TROPOMI: First results and a comparison with ECMWF-IFS analysis data.  
903 *Geophysical Research Letters*, 45(6), 2826-2832.  
904  
905 Borsdorff, T., Campos, T., Kille, N., Zarzana, K. J., Volkamer, R., and Landgraf, J.: Vertical  
906 information of CO from TROPOMI total column measurements in context of the CAMS-IFS data  
907 assimilation scheme, *Atmos. Meas. Tech.*, 16, 3027–3038, [https://doi.org/10.5194/amt-16-3027-](https://doi.org/10.5194/amt-16-3027-2023)  
908 [2023](https://doi.org/10.5194/amt-16-3027-2023), 2023.  
909  
910 [Buschmann, M., Petri, C., Palm, M., Warneke, T., & Notholt, J.: TCCON data from Ny-Ålesund,](https://doi.org/10.14291/tccon.ggg2020.nyalesund01.R0)  
911 [Svalbard \(NO\), Release GGG2020.R0 \(Version R0\) \[Data set\].](https://doi.org/10.14291/tccon.ggg2020.nyalesund01.R0)  
912 [CaltechDATA. https://doi.org/10.14291/tccon.ggg2020.nyalesund01.R0, 2022.](https://doi.org/10.14291/tccon.ggg2020.nyalesund01.R0)  
913  
914 Candille, G., Côté, C., Houtekamer, P.L. and Pellerin, G.: Verification of an ensemble prediction  
915 system against observations. *Monthly Weather Review*, 135(7), pp.2688-2699, 2007.  
916  
917 Chance, K., Liu, X., Miller, C. C., González Abad, G., Huang, G., Nowlan, C., Souri, A., Suleiman,  
918 R., Sun, K., Wang, H., Zhu, L., Zoogman, P., Al-Saadi, J., Antuña-Marrero, J. C., Carr, J.,  
919 Chatfield, R., Chin, M., Cohen, R., Edwards, D., Fishman, J., Flittner, D., Geddes, J., Grutter, M.,  
920 Herman, J. R., Jacob, D. J., Janz, S., Joiner, J., Kim, J., Krotkov, N. A., Lefer, B., Martin, R. V.,  
921 Mayol-Bracero, O. L., Naeger, A., Newchurch, M., Pfister, G. G., Pickering, K., Pierce, R. B.,  
922 Rivera Cárdenas, C., Saiz-Lopez, A., Simpson, W., Spinei, E., Spurr, R. J. D., Szykman, J. J.,  
923 Torres, O., and Wang, J.: TEMPO Green Paper: Chemistry, Physics, and Meteorology  
924 Experiments with the Tropospheric Emissions: Monitoring of Pollution Instrument, in: *Sensors,*  
925 *Systems, and Next-Generation Satellites XXIII*, Strasbourg, France, 9-12 September 2019, edited  
926 by: Neeck, S. P., Kimura, T., and Martimort, P., *Proc. SPIE*, 11151, p.10,  
927 <https://doi.org/10.1117/12.2534883>, 2019.  
928



929 Cuesta, J., Eremenko, M., Liu, X., Dufour, G., Cai, Z., Höpfner, M., von Clarmann, T., Sellitto,  
930 P., Forêt, G., Gaubert, B. and Beekmann, M., 2013. Satellite observation of lowermost  
931 tropospheric ozone by multispectral synergism of IASI thermal infrared and GOME-2 ultraviolet  
932 measurements over Europe. *Atmospheric Chemistry and Physics*, 13(19), pp.9675-9693.  
933  
934 Danabasoglu, G., Lamarque, J.F., Bacmeister, J., Bailey, D.A., DuVivier, A.K., Edwards, J.,  
935 Emmons, L.K., Fasullo, J., Garcia, R., Gettelman, A. and Hannay, C., 2020. The community earth  
936 system model version 2 (CESM2). *Journal of Advances in Modeling Earth Systems*, 12(2),  
937 p.e2019MS001916.  
938  
939 Deeter, M. N., Emmons, L. K., Francis, G. L., Edwards, D. P., Gille, J. C., Warner, J. X., Khattatov,  
940 B., Ziskin, D., Lamarque, J.-F., Ho, S.-P., Yudin, V., Attie, J.-L., Packman, D., Chen, J., Mao, D.,  
941 and Drummond, J. R.: Operational carbon monoxide retrieval algorithm and selected results for  
942 the MOPITT instrument, *J. Geophys. Res.*, 108(D14), 4399, doi:10.1029/2002JD003186, 2003.  
943  
944 Deeter, M. N., Worden, H. M., Gille, J. C., Edwards, D. P., Mao, D., and Drummond, J. R.:  
945 MOPITT multispectral CO retrievals: Origins and effects of geophysical radiance errors, *J.*  
946 *Geophys. Res.*, 116, D15303, doi:10.1029/2011JD015703, 2011.  
947  
948 Deeter, M. N., Martínez-Alonso, S., Edwards, D. P., Emmons, L. K., Gille, J. C., Worden, H. M.,  
949 Pittman, J. V., Daube, B. C., and Wofsy, S. C.: Validation of MOPITT Version 5 thermalinfrared,  
950 near-infrared, and multispectral carbon monoxide profile retrievals for 2000–2011, *J. Geophys.*  
951 *Res.*, 118, 6710–6725, doi:10.1002/jgrd.50272, 2013.  
952  
953 Deeter, M., Francis, G., Gille, J., Mao, D., Martínez-Alonso, S., Worden, H., Ziskin, D.,  
954 Drummond, J., Commane, R., Diskin, G., and McKain, K.: The MOPITT Version 9 CO product:  
955 sampling enhancements and validation, *Atmos. Meas. Tech.*, 15, 2325–2344,  
956 <https://doi.org/10.5194/amt-15-2325-2022>, 2022.  
957  
958 Emmons, L. K., Schwantes, R. H., Orlando, J. J., Tyndall, G., Kinnison, D., Lamarque, J.-F., et al.  
959 (2020). The chemistry mechanism in the Community Earth System Model version 2 (CESM2).  
960 *Journal of Advances in Modeling Earth Systems*, 12(4), e2019MS001882.  
961 <https://doi.org/10.1029/2019MS001882>.  
962  
963 Flynn, L., et al. (2014), Performance of the Ozone Mapping and Profiler Suite (OMPS) products,  
964 *J. Geophys. Res. Atmos.*, 119, 6181–6195, doi:10.1002/2013JD020467.  
965  
966 Fu, D., Bowman, K. W., Worden, H. M., Natraj, V., Worden, J. R., Yu, S., Veeffkind, P., Aben, I.,  
967 Landgraf, J., Strow, L., and Han, Y.: High-resolution tropospheric carbon monoxide profiles  
968 retrieved from CrIS and TROPOMI, *Atmos. Meas. Tech.*, 9, 2567–2579,  
969 <https://doi.org/10.5194/amt-9-2567-2016>, 2016.  
970  
971 Fu, D., Kulawik, S. S., Miyazaki, K., Bowman, K. W., Worden, J. R., Eldering, A., Livesey, N. J.,  
972 Teixeira, J., Irion, F. W., Herman, R. L., Osterman, G. B., Liu, X., Levelt, P. F., Thompson, A.  
973 M., and Luo, M.: Retrievals of tropospheric ozone profiles from the synergism of AIRS and OMI:

974 methodology and validation, *Atmos. Meas. Tech.*, 11, 5587–5605, [https://doi.org/10.5194/amt-11-](https://doi.org/10.5194/amt-11-5587-2018)  
975 5587-2018, 2018.

976  
977 [García, O. E., Schneider, M., Herkommer, B., Gross, J., Hase, F., Blumenstock, T., & Sepúlveda,](https://doi.org/10.14291/tccon.ggg2020.izana01.R1.2022)  
978 [E. \(2022\). TCCON data from Izana \(ES\), Release GGG2020.R1 \(Version R1\) \[Data set\].](https://doi.org/10.14291/tccon.ggg2020.izana01.R1.2022)  
979 [CaltechDATA. https://doi.org/10.14291/tccon.ggg2020.izana01.R1.2022.](https://doi.org/10.14291/tccon.ggg2020.izana01.R1.2022)  
980

981 [Gaspari, G., and S. E. Cohn, 1999: Construction of correlation functions in two and three](https://doi.org/10.1002/qj.49712555417)  
982 [dimensions. \*Quart. J. Roy. Meteor. Soc.\*, 125, 723–757, https://doi.org/10.1002/qj.49712555417.](https://doi.org/10.1002/qj.49712555417)  
983

984 Gaubert, B., Coman, A., Foret, G., Meleux, F., Ung, A., Rouil, L., Ionescu, A., Candau, Y., and  
985 Beekmann, M.: Regional scale ozone data assimilation using an ensemble Kalman filter and the  
986 CHIMERE chemical transport model, *Geosci. Model Dev.*, 7, 283–302,  
987 <https://doi.org/10.5194/gmd-7-283-2014>, 2014.

988  
989 Gaubert, B., Arellano, A. F., Barré, J., Worden, H. M., Emmons, L. K., Tilmes, S., Buchholz, R.  
990 R., Vitt, F., Raeder, K., Collins, N., Anderson, J. L., Wiedinmyer, C., Martínez-Alonso, S.,  
991 Edwards, D. P., Andreae, M. O., Hannigan, J. W., Petri, C., Strong, K., and Jones, N.: Toward a  
992 chemical reanalysis in a coupled chemistry-climate model: An evaluation of MOPITT CO  
993 assimilation and its impact on tropo- spheric composition, *J. Geophys. Res.-Atmos.*, 121, 7310–  
994 7343, <https://doi.org/10.1002/2016JD024863>, 2016.

995  
996 Gaubert, B., Worden, H. M., Arellano, A. F. J., Emmons, L. K., Tilmes, S., Barré, J., Martinez  
997 Alonso, S., Vitt, F., Anderson, J. L., Alkemade, F., Houweling, S., and Ed-  
998 wards, D. P.: Chemical feedback from decreasing carbon monoxide emissions. *Geophys. Res. Lett.*, 44, 9985–9995,  
999 <https://doi.org/10.1002/2017GL074987>, 2017.

1000  
1001 Gaubert, B., Emmons, L. K., Raeder, K., Tilmes, S., Miyazaki, K., Arellano Jr., A. F., Elguindi,  
1002 N., Granier, C., Tang, W., Barré, J., Worden, H. M., Buchholz, R. R., Edwards, D. P., Franke, P.,  
1003 Anderson, J. L., Saunio, M., Schroeder, J., Woo, J.-H., Simpson, I. J., Blake, D. R., Meinardi, S.,  
1004 Wennberg, P. O., Crouse, J., Teng, A., Kim, M., Dickerson, R. R., He, H., Ren, X., Pusede, S.  
1005 E., and Diskin, G. S.: Correcting model biases of CO in East Asia: impact on oxidant distributions  
1006 during KORUS-AQ, *Atmos. Chem. Phys.*, 20, 14617–14647, [https://doi.org/10.5194/acp-20-](https://doi.org/10.5194/acp-20-14617-2020)  
1007 14617-2020, 2020.

1008  
1009 Gaubert, B., Edwards, D. P., Anderson, J. L., Arellano, A.F., Barré, J., Buchholz, R.R., Darras, S.,  
1010 Emmons, L.K., Fillmore, D., Granier, C., et al. Global Scale Inversions from MOPITT CO and  
1011 MODIS AOD. *Remote Sens.* 2023,15,4813. <https://doi.org/10.3390/rs15194813>.

1012  
1013 [Hase, F., Herkommer, B., Groß, J., Blumenstock, T., Kiel, M. ä ., & Dohe, S.: TCCON data from](https://doi.org/10.14291/tccon.ggg2020.karlsruhe01.R0.2022)  
1014 [Karlsruhe \(DE\), Release GGG2020.R0 \(Version R0\) \[Data set\]. CaltechDATA.](https://doi.org/10.14291/tccon.ggg2020.karlsruhe01.R0.2022)  
1015 [https://doi.org/10.14291/tccon.ggg2020.karlsruhe01.R0.2022.](https://doi.org/10.14291/tccon.ggg2020.karlsruhe01.R0.2022)  
1016

1017 [Hedelius, J. K., He, T.-L., Jones, D. B. A., Baier, B. C., Buchholz, R. R., De Mazière, M.,](https://doi.org/10.1029/2017JD026881)  
1018 [Deutscher, N. M., Dubey, M. K., Feist, D. G., Griffith, D. W. T., Hase, F., Iraci, L. T., Jeseck, P.,](https://doi.org/10.1029/2017JD026881)  
1019 [Kiel, M., Kivi, R., Liu, C., Morino, I., Notholt, J., Oh, Y.-S., Ohyama, H., Pollard, D. F., Rettinger,](https://doi.org/10.1029/2017JD026881)

1020 [M., Roche, S., Roehl, C. M., Schneider, M., Shiomi, K., Strong, K., Sussmann, R., Sweeney, C.,](#)  
1021 [Té, Y., Uchino, O., Velasco, V. A., Wang, W., Warneke, T., Wennberg, P. O., Worden, H. M.,](#)  
1022 [and Wunch, D.: Evaluation of MOPITT Version 7 joint TIR–NIR XCO retrievals with TCCON,](#)  
1023 [Atmos. Meas. Tech., 12, 5547–5572, <https://doi.org/10.5194/amt-12-5547-2019>, 2019.](#)  
1024  
1025 Inness, A., M. Ades, A. Agustí-Panareda, J. Barré, A. Benedictow, A.-M. Blechschmidt, J. J.  
1026 Dominguez, R. Engelen, H. Eskes, J. Flemming, V. Huijnen, L. Jones, Z. Kipling, S. Massart, M.  
1027 Parrington, V.-H. Peuch, M. Razinger, S. Remy, M. Schulz, and M. Suttie (2019), The CAMS  
1028 reanalysis of atmospheric composition, *Atmospheric Chemistry and Physics*, 19(6), 35153556,  
1029 <https://doi.org/10.5194/acp-19-3515-2019>.  
1030  
1031 Inness, A., I. Aben, M. Ades, T. Borsdorff, J. Flemming, L. Jones, J. Landgraf, B. Langerock, P.  
1032 Nedelec, M. Parrington, and R. Ribas (2022), Assimilation of S5P/TROPOMI carbon monoxide  
1033 data with the global CAMS near-real-time system, *Atmospheric Chemistry and Physics*, 22(21),  
1034 1435514376, doi:[10.5194/acp-22-14355-2022](https://doi.org/10.5194/acp-22-14355-2022).  
1035  
1036 [Iraci, L. T., Podolske, J. R., Roehl, C., Wennberg, P. O., Blavier, J.-F., Allen, N., Wunch, D., &](#)  
1037 [Osterman, G. B.: TCCON data from Edwards \(US\), Release GGG2020.R0 \(Version R0\) \[Data](#)  
1038 [set\]. CaltechDATA. <https://doi.org/10.14291/tcon.ggg2020.edwards01.R0, 2022>.](#)  
1039  
1040 Jiang, Z., Jones, D. B. A., Worden, H. M., Deeter, M. N., Henze, D. K., Worden, J., Bowman, K.  
1041 W., Brenninkmeijer, C. A. M., and Schuck, T. J.: Impact of model errors in convective transport  
1042 on CO source estimates inferred from MOPITT CO retrievals, *J. Geophys. Res.-Atmos.*, 118,  
1043 2073–2083, <https://doi.org/10.1002/jgrd.50216>, 2013.  
1044  
1045 Jiang, Z., Worden, J. R., Worden, H., Deeter, M., Jones, D. B. A., Arellano, A. F., and Henze, D.  
1046 K.: A 15-year record of CO emissions constrained by MOPITT CO observations, *Atmos. Chem.*  
1047 *Phys.*, 17, 4565–4583, <https://doi.org/10.5194/acp-17-4565-2017>, 2017.  
1048  
1049 Kim, J., Jeong, U., Ahn, M.-H., Kim, J. H., Park, R. J., Lee, H., Song, C. H., Choi, Y.-S., Lee, K.-  
1050 H., Yoo, J.-M., Jeong, M.-J., Park, S. K., Lee, K.-M., Song, C.-K., Kim, S.-W., Kim, Y. J., Kim,  
1051 S.-W., Kim, M., Go, S., Liu, X., Chance, K., Chan Miller, C., Al-Saadi, J., Veihelmann, B.,  
1052 Bhartia, P. K., Torres, O., Abad, G. G., Haffner, D. P., Ko, D. H., Lee, S. H., Woo, J.-H., Chong,  
1053 H., Park, S. S., Nicks, D., Choi, W. J., Moon, K.-J., Cho, A., Yoon, J., Kim, S.-k., Hong, H., Lee,  
1054 K., Lee, H., Lee, S., Choi, M., Veefkind, P., Levelt, P. F., Edwards, D. P., Kang, M., Eo, M., Bak,  
1055 J., Baek, K., Kwon, H.-A., Yang, J., Park, J., Han, K. M., Kim, B.-R., Shin, H.-W., Choi, H., Lee,  
1056 E., Chong, J., Cha, Y., Koo, J.-H., Irie, H., Hayashida, S., Kasai, Y., Kanaya, Y., Liu, C., Lin, J.,  
1057 Crawford, J. H., Carmichael, G. R., Newchurch, M. J., Lefer, B. L., Herman, J. R., Swap, R. J.,  
1058 Lau, A. K. H., Kurosu, T. P., Jaross, G., Ahlers, B., Dobber, M., McElroy, C. T., and Choi, Y.:  
1059 New Era of Air Quality Monitoring from Space: Geostationary Environment Monitoring  
1060 Spectrometer (GEMS), *B. Am. Meteorol. Soc.*, 101, E1–E22, [https://doi.org/10.1175/bams-d-18-](https://doi.org/10.1175/bams-d-18-0013.1)  
1061 [0013.1](https://doi.org/10.1175/bams-d-18-0013.1), 2020.  
1062  
1063 [Kivi, R., Heikkinen, P., & Kyrö, E.: TCCON data from Sodankylä \(FI\), Release GGG2020.R0](#)  
1064 [\(Version R0\) \[Data set\]. CaltechDATA. \[https://doi.org/10.14291/tcon.ggg2020.sodankyla01.R0,\]\(https://doi.org/10.14291/tcon.ggg2020.sodankyla01.R0, 2022\)](#)  
1065 [2022](https://doi.org/10.14291/tcon.ggg2020.sodankyla01.R0, 2022).

Deleted: ¶

1067  
1068 [Kopacz, M., Breeze, V., Kondragunta, S., Frost, G., Anenberg, S., Bruhwiler, L., Davis, S., da](#)  
1069 [Silva, A., de Gouw, J., Duren, R. and Flynn, L., Global Atmospheric Composition Needs from](#)  
1070 [Future Ultraviolet–Visible–Near-Infrared \(UV–Vis–NIR\) NOAA Satellite Instruments. \*Bulletin\*](#)  
1071 [of the American Meteorological Society](#), 104(3), pp. E623–E630, 2023,  
1072 <https://doi.org/10.1175/BAMS-D-22-0266.1>  
1073  
1074 [Laughner, J. L., Toon, G. C., Mendonca, J., Petri, C., Roche, S., Wunch, D., Blavier, J.-F., Griffith,](#)  
1075 [D. W. T., Heikkinen, P., Keeling, R. F., Kiel, M., Kivi, R., Roehl, C. M., Stephens, B. B., Baier,](#)  
1076 [B. C., Chen, H., Choi, Y., Deutscher, N. M., DiGangi, J. P., Gross, J., Herkommer, B., Jeseck, P.,](#)  
1077 [Laemmel, T., Lan, X., McGee, E., McKain, K., Miller, J., Morino, I., Notholt, J., Ohyama, H.,](#)  
1078 [Pollard, D. F., Rettinger, M., Riris, H., Rousogenuous, C., Sha, M. K., Shiomi, K., Strong, K.,](#)  
1079 [Sussmann, R., Té, Y., Velazco, V. A., Wofsy, S. C., Zhou, M., and Wennberg, P. O.: The Total](#)  
1080 [Carbon Column Observing Network's GGG2020 Data Version. \*Earth Syst. Sci. Data Discuss.\*](#)  
1081 [\[preprint\], <https://doi.org/10.5194/essd-2023-331>, in review, 2023.](#)  
1082  
1083 Levelt, P. F., Joiner, J., Tamminen, J., Veefkind, J. P., Bhartia, P. K., Stein Zweers, D. C., Duncan,  
1084 B. N., Streets, D. G., Eskes, H., van der A, R., McLinden, C., Fioletov, V., Carn, S., de Laat, J.,  
1085 DeLand, M., Marchenko, S., McPeters, R., Ziemke, J., Fu, D., Liu, X., Pickering, K., Apituley,  
1086 A., González Abad, G., Arola, A., Boersma, F., Chan Miller, C., Chance, K., de Graaf, M.,  
1087 Hakkarainen, J., Hassinen, S., Ialongo, I., Kleipool, Q., Krotkov, N., Li, C., Lamsal, L., Newman,  
1088 P., Nowlan, C., Suleiman, R., Tilstra, L. G., Torres, O., Wang, H., and Wargan, K.: The Ozone  
1089 Monitoring Instrument: overview of 14 years in space, *Atmos. Chem. Phys.*, 18, 5699–5745,  
1090 <https://doi.org/10.5194/acp-18-5699-2018>, 2018.  
1091  
1092 Liu, X., Ma, P.-L., Wang, H., Tilmes, S., Singh, B., Easter, R. C., et al. (2016b). Description and  
1093 evaluation of a new four-mode version of the Modal Aerosol Module (MAM4) within version 5.3  
1094 of the Community Atmosphere Model. *Geoscientific Model Development*, 9, 505–522.  
1095 <https://doi.org/10.5194/gmd-9-505-2016>.  
1096  
1097 [Liu, C., Wang, W., Sun, Y., & Shan, C.: TCCON data from Hefei \(PRC\), Release GGG2020.R0](#)  
1098 [\(Version R0\) \[Data set\]. CaltechDATA. <https://doi.org/10.14291/tcon.ggg2020.hefei01.R0>,](#)  
1099 [2022.](#)  
1100  
1101 [Martínez-Alonso, S., Deeter, M., Worden, H., Borsdorff, T., Aben, I., Commane, R., Daube, B.,](#)  
1102 [Francis, G., George, M., Landgraf, J. and Mao, D., 2020. 1.5 years of TROPOMI CO](#)  
1103 [measurements: comparisons to MOPITT and ATom. \*Atmospheric Measurement Techniques\*,](#)  
1104 [13\(9\), pp.4841–4864.](#)  
1105  
1106 Ménard, R. and Chang, L.P.: Assimilation of stratospheric chemical tracer observations using a  
1107 Kalman filter. Part II:  $\chi^2$ -validated results and analysis of variance and correlation dynamics.  
1108 *Monthly weather review*, 128(8), pp.2672–2686, [https://doi.org/10.1175/1520-](https://doi.org/10.1175/1520-0493(2000)128<2672:AOSCTO>2.0.CO;2)  
1109 [0493\(2000\)128<2672:AOSCTO>2.0.CO;2](https://doi.org/10.1175/1520-0493(2000)128<2672:AOSCTO>2.0.CO;2), 2000.  
1110  
1111 Mettig, N., Weber, M., Rozanov, A., Burrows, J. P., Veefkind, P., Thompson, A. M., Stauffer, R.  
1112 M., Leblanc, T., Ancellet, G., Newchurch, M. J., Kuang, S., Kivi, R., Tully, M. B., Van Malderen,

Formatted: Left, Font Alignment: Bottom, Pattern: Clear (White)

Formatted: Font color: Black

1113 R., Piders, A., Kois, B., Stübi, R., and Skrivankova, P.: Combined UV and IR ozone profile  
1114 retrieval from TROPOMI and CrIS measurements, *Atmos. Meas. Tech.*, 15, 2955–2978,  
1115 <https://doi.org/10.5194/amt-15-2955-2022>, 2022.

1116  
1117 [Morino, I., Ohyama, H., Hori, A., & Ikegami, H.: TCCON data from Rikubetsu \(JP\), Release  
1118 GGG2020.R0 \(Version R0\) \[Data set\]. CaltechDATA.  
1119 <https://doi.org/10.14291/tcon.ggg2020.rikubetsu01.R0>, 2022a.](https://doi.org/10.14291/tcon.ggg2020.rikubetsu01.R0)

1120  
1121 [Morino, I., Ohyama, H., Hori, A., & Ikegami, H.: TCCON data from Tsukuba \(JP\), 125HR,  
1122 Release GGG2020.R0 \(Version R0\) \[Data set\]. CaltechDATA.  
1123 <https://doi.org/10.14291/tcon.ggg2020.tsukuba02.R0>, 2022b.](https://doi.org/10.14291/tcon.ggg2020.tsukuba02.R0)

1124  
1125 [Morino, I., Velazco, V. A., Hori, A., Uchino, O., & Griffith, D. W. T.: TCCON data from Burgos,  
1126 Ilocos Norte \(PH\), Release GGG2020.R0 \(Version R0\) \[Data set\]. CaltechDATA.  
1127 <https://doi.org/10.14291/tcon.ggg2020.burgos01.R0>, 2022c.](https://doi.org/10.14291/tcon.ggg2020.burgos01.R0)

1128  
1129 Natraj V., X. Liu, S. Kulawik, K. Chance, R. Chatfield, D.P. Edwards, A. Eldering, G. Francis, T.  
1130 Kurosu, K. Pickering, R. Spurr, and H. M. Worden. Multi-spectral sensitivity studies for the  
1131 retrieval of tropospheric and lowermost tropospheric ozone from simulated clear-sky geo-cape  
1132 measurements *Atmos. Environ.*, 45, 7151-7165. <https://doi.org/10.1016/j.atmosenv.2011.09.014>,  
1133 2011.

1134  
1135 [Notholt, J., Petri, C., Warneke, T., & Buschmann, M.: TCCON data from Bremen \(DE\), Release  
1136 GGG2020.R0 \(Version R0\) \[Data set\]. CaltechDATA.  
1137 <https://doi.org/10.14291/tcon.ggg2020.bremen01.R0>, 2022.](https://doi.org/10.14291/tcon.ggg2020.bremen01.R0)

1138  
1139 Petron, G., Crotwell, A.M., Crotwell, M.J., Dlugokencky, E., Madronich, M., Moglia, E., Neff,  
1140 D., Thoning, K., Wolter, S., Mund, J.W. (2022), Atmospheric Carbon Monoxide Dry Air Mole  
1141 Fractions from the NOAA GML Carbon Cycle Cooperative Global Air Sampling Network, 1988-  
1142 2021, Version: 2022-07-28, <https://doi.org/10.15138/33bv-s284>.

1143  
1144 Peuch, V. H., Engelen, R., Rixen, M., Dee, D., Flemming, J., Suttie, M., ... & Thépaut, J. N. (2022).  
1145 The copernicus atmosphere monitoring service: From research to operations. *Bulletin of the  
1146 American Meteorological Society*, 103(12), E2650-E2668. [https://doi.org/10.1175/BAMS-D-21-  
1147 0314.1](https://doi.org/10.1175/BAMS-D-21-0314.1)

1148  
1149 Pfister, G., Eastham, S., Arellano, A. F., Aumont, B., Barsanti, K., Barth, M., Conley, A., Davis,  
1150 N., Emmons, L., Fast, J., Fiore, A., Gaubert, B., Goldhaber, S., Granier, C., Grell, G., Guevara,  
1151 M., Henze, D., Hodzic, A., Liu, X., Marsh, D., Orlando, J., Plane, J., Polvani, L., Rosenlof, K.,  
1152 Steiner, A., Jacob, D., and Brasseur, G.: The Multi-Scale Infrastructure for Chemistry and Aerosols  
1153 (MUSICA), *B. Am. Meteorol. Soc.*, 101, E1743–E1760, [https://doi.org/10.1175/bams-d-19-  
1154 0331.1](https://doi.org/10.1175/bams-d-19-0331.1), 2020.

1155  
1156 Petzold, A., Thouret, V., Gerbig, C., Zahn, A., Brenninkmeijer, C.A., Gallagher, M., Hermann,  
1157 M., Pontaud, M., Ziereis, H., Boulanger, D. and Marshall, J., 2015. Global-scale atmosphere

1158 monitoring by in-service aircraft—current achievements and future prospects of the European  
1159 Research Infrastructure IAGOS. *Tellus B: Chemical and Physical Meteorology*, 67(1), p.28452.

1160  
1161 [Pollard, D. F., Robinson, J., & Shiona, H.: TCCON data from Lauder \(NZ\), Release GGG2020.R0  
1162 \(Version R0\) \[Data set\]. CaltechDATA. \[https://doi.org/10.14291/tcon.ggg2020.lauder03.R0,  
1163 2022.\]\(https://doi.org/10.14291/tcon.ggg2020.lauder03.R0.2022\)](https://doi.org/10.14291/tcon.ggg2020.lauder03.R0.2022)

1164  
1165 Raeder, K, J. L., Anderson, N. Collins, T. J. Hoar, J. E. Kay, P. H., Lauritzen and R. Pincus, 2012  
1166 DART/CAM: An Ensemble Data Assimilation for CESM Atmospheric Models. *Journal of  
1167 Climate*, 25, 6304-6317, doi:10.1175/JCLI-D-11-00395.1.

1168  
1169 Raeder, K., Hoar, T. J., El-Gharamti, M., Johnson, B. K., Collins, N., Anderson, J. L., Steward, J.,  
1170 Coady, M. A new CAM6 + DART reanalysis with surface forcing from CAM6 to other CESM  
1171 models. *Scientific Reports* 2021, 11. [https://doi.org/10.1038/s41598-078521-92927-0.](https://doi.org/10.1038/s41598-078521-92927-0)

1172  
1173 [Rodgers, C.D., 2000. Inverse Methods for Atmospheric Sounding: Theory and Practice, World  
1174 Scientific Publishing Co. Ltd, London, UK, 238pp.](#)

1175  
1176 Schneider, M., Ertl, B., Tu, Q., Diekmann, C.J., Khosrawi, F., Röhling, A.N., Hase, F., Dubravica,  
1177 D., García, O.E., Sepúlveda, E. and Borsdorff, T., 2022. Synergetic use of IASI profile and  
1178 TROPOMI total-column level 2 methane retrieval products. *Atmospheric Measurement  
1179 Techniques*, 15(14), pp.4339-4371.

1180  
1181 Sekiya, T., Miyazaki, K., Ogochi, K., Sudo, K., Takigawa, M., Eskes, H. and Boersma, K.F., 2021.  
1182 Impacts of horizontal resolution on global data assimilation of satellite measurements for  
1183 tropospheric chemistry analysis. *Journal of Advances in Modeling Earth Systems*, 13(6),  
1184 p.e2020MS002180.

1185  
1186 [Shiomi, K., Kawakami, S., Ohyama, H., Arai, K., Okumura, H., Ikegami, H., & Usami, M.:  
1187 TCCON data from Saga \(JP\), Release GGG2020.R0 \(Version R0\) \[Data set\].  
1188 CaltechDATA. \[https://doi.org/10.14291/tcon.ggg2020.saga01.R0, 2022.\]\(https://doi.org/10.14291/tcon.ggg2020.saga01.R0.2022\)](https://doi.org/10.14291/tcon.ggg2020.saga01.R0.2022)

1189  
1190 Soulie, A., C. Granier, S. Darras, N. Zilbermann, T. Doumbia, M. Guevara, J.-P. Jalkanen, S.  
1191 Keita, C. Lioussé, M. Crippa, D. Guizzardi, R. Hoesly, S. J. Smith, Global Anthropogenic  
1192 Emissions (CAM5-GLOB-ANT) for the Copernicus Atmosphere Monitoring Service Simulations  
1193 of Air Quality Forecasts and Reanalyses, submitted to *Earth Syst. Sci. Data*, paper esd-2023-306,  
1194 2023.

1195  
1196 Tang, W., Emmons, L.K., Buchholz, R.R., Wiedinmyer, C., Schwantes, R.H., He, C., Kumar, R.,  
1197 Pfister, G.G., Worden, H.M., Hornbrook, R.S. and Apel, E.C., 2022. Effects of fire diurnal  
1198 variation and plume rise on US Air quality during FIREX-AQ and WE-CAN Based on the multi-  
1199 scale infrastructure for chemistry and aerosols (MUSICAv0). *Journal of Geophysical Research:  
1200 Atmospheres*, 127(16), p.e2022JD036650.

1201  
1202 Tang, W., Pfister, G.G., Kumar, R., Barth, M., Edwards, D.P., Emmons, L.K. and Tilmes, S., 2023.  
1203 Capturing High-Resolution Air Pollution Features Using the Multi-Scale Infrastructure for

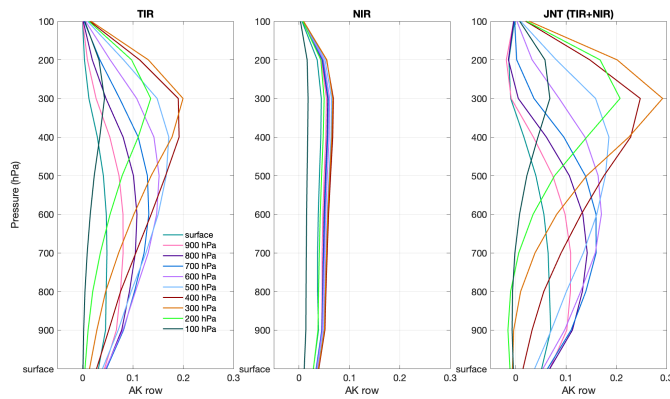
1204 Chemistry and Aerosols Version 0 (MUSICAv0) Global Modeling System. Journal of  
1205 Geophysical Research: Atmospheres, 128(7), p.e2022JD038345.  
1206  
1207 [Té, Y., Jeseck, P., & Janssen, C.: TCCON data from Paris \(FR\), Release GGG2020.R0 \(Version](https://doi.org/10.14291/tccon.ggg2020.paris01.R0)  
1208 [R0\) \[Data set\]. CaltechDATA. https://doi.org/10.14291/tccon.ggg2020.paris01.R0, 2022.](https://doi.org/10.14291/tccon.ggg2020.paris01.R0)  
1209  
1210 Total Carbon Column Observing Network (TCCON) Team. (2022). 2020 TCCON Data Release  
1211 (Version GGG2020) [Data set]. CaltechDATA. <https://doi.org/10.14291/TCCON.GGG2020>.  
1212  
1213 Tilmes, S., Hodzic, A., Emmons, L. K., Mills, M. J., Gettelman, A., Kinnison, D. E., et al. (2019).  
1214 Climate forcing and trends of organic aerosols in the Community Earth System Model (CESM2).  
1215 Journal of Advances in Modeling Earth Systems, 11(12), 4323–4351.  
1216 <https://doi.org/10.1029/2019MS00182>.  
1217  
1218 Total Carbon Column Observing Network (TCCON) Team. (2022). 2020 TCCON Data Release  
1219 (Version GGG2020) [Data set]. CaltechDATA. <https://doi.org/10.14291/TCCON.GGG2020>.  
1220  
1221 Veeffkind, J. P., Aben, I., McMullan, K., Förster, H., De Vries, J., Otter, G., ... & Levelt, P. F.  
1222 (2012). TROPOMI on the ESA Sentinel-5 Precursor: A GMES mission for global observations of  
1223 the atmospheric composition for climate, air quality and ozone layer applications. Remote Sensing  
1224 of Environment, 120, 70-83.  
1225  
1226 [Warneke, T., Petri, C., Notholt, J., & Buschmann, M.: TCCON data from Orléans \(FR\), Release](https://doi.org/10.14291/tccon.ggg2020.orleans01.R0)  
1227 [GGG2020.R0 \(Version R0\) \[Data set\].](https://doi.org/10.14291/tccon.ggg2020.orleans01.R0)  
1228 [CaltechDATA. https://doi.org/10.14291/tccon.ggg2020.orleans01.R0, 2022.](https://doi.org/10.14291/tccon.ggg2020.orleans01.R0)  
1229  
1230 [Wennberg, P. O., Roehl, C. M., Wunch, D., Toon, G. C., Blavier, J.-F., Washenfelder, R., Keppel-](https://doi.org/10.14291/tccon.ggg2020.parkfalls01.R1)  
1231 [Aleks, G., & Allen, N. T.: TCCON data from Park Falls \(US\), Release GGG2020.R1 \(Version R1\)](https://doi.org/10.14291/tccon.ggg2020.parkfalls01.R1)  
1232 [\[Data set\]. CaltechDATA. https://doi.org/10.14291/tccon.ggg2020.parkfalls01.R1, 2022a.](https://doi.org/10.14291/tccon.ggg2020.parkfalls01.R1)  
1233  
1234 [Wennberg, P. O., Wunch, D., Roehl, C. M., Blavier, J.-F., Toon, G. C., & Allen, N. T.: TCCON](https://doi.org/10.14291/tccon.ggg2020.lamont01.R0)  
1235 [data from Lamont \(US\), Release GGG2020.R0 \(Version R0\) \[Data set\].](https://doi.org/10.14291/tccon.ggg2020.lamont01.R0)  
1236 [CaltechDATA. https://doi.org/10.14291/tccon.ggg2020.lamont01.R0, 2022b.](https://doi.org/10.14291/tccon.ggg2020.lamont01.R0)  
1237  
1238 Wiedinmyer, C., Kimura, Y., McDonald-Buller, E. C., Emmons, L. K., Buchholz, R. R., Tang,  
1239 W., Seto, K., Joseph, M. B., Barsanti, K. C., Carlton, A. G., and Yokelson, R.: The Fire Inventory  
1240 from NCAR version 2.5: an updated global fire emissions model for climate and chemistry  
1241 applications, Geosci. Model Dev., 16, 3873–3891, <https://doi.org/10.5194/gmd-16-3873-2023>,  
1242 2023.  
1243  
1244 Worden, H.M., Logan, J.A., Worden, J.R., Beer, R., Bowman, K., Clough, S.A., Eldering, A.,  
1245 Fisher, B.M., Gunson, M.R., Herman, R.L. and Kulawik, S.S., 2007. Comparisons of Tropospheric  
1246 Emission Spectrometer (TES) ozone profiles to ozonesondes: Methods and initial results. Journal  
1247 of Geophysical Research: Atmospheres, 112(D3).  
1248

1249 Worden, H. M., Deeter, M. N., Edwards, D. P., Gille, J. C., Drummond, J. R., and Nédélec, P.:  
1250 Observations of near-surface carbon monoxide from space using MOPITT multispectral retrievals,  
1251 J. Geophys. Res., 115, D18314, <https://doi.org/10.1029/2010JD014242>, 2010.

1252  
1253 [Wunch, D., G. C. Toon, J.-F. L. Blavier, R. A. Washenfelder, J. Notholt, B. J. Connor, D. W. T. Griffith, V. Sherlock, and P. O. Wennberg: The Total Carbon Column Observing Network, Philos. Trans. R. Soc. A Math. Phys. Eng. Sci., 369\(1943\), 2087–2112, doi:10.1098/rsta.2010.0240, 2011.](#)

1257 [Wunch, D., Mendonca, J., Colebatch, O., Allen, N. T., Blavier, J.-F., Kunz, K., Roche, S., Hedelius, J., Neufeld, G., Springett, S., Worthy, D., Kessler, R., & Strong, K.: TCCON data from East Trout Lake, SK \(CA\), Release GGG2020.R0 \(Version R0\) \[Data set\]. CaltechDATA, <https://doi.org/10.14291/tcon.ggg2020.easttroutlake01.R0>, 2022.](#)

1261  
1262 Zeng, Z.-C., Lee, L., and Qi, C.: Diurnal carbon monoxide observed from a geostationary infrared  
1263 hyperspectral sounder: first result from GIIRS on board FengYun-4B, Atmos. Meas. Tech., 16,  
1264 3059–3083, <https://doi.org/10.5194/amt-16-3059-2023>, 2023.



1272 **Figure 1.** Averaging kernel (AK) rows for MOPITT retrieval types TIR only, NIR only, and  
1273 multispectral TIR+NIR. Global average of AKs during July and August 2018 are shown.

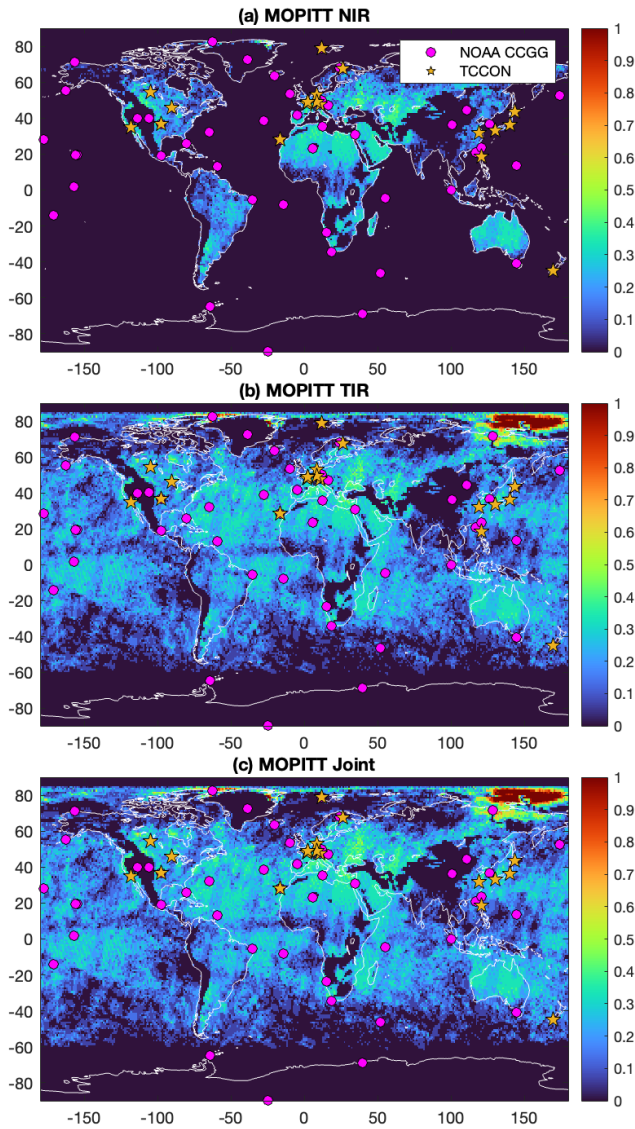
Formatted: Left, Font Alignment: Bottom, Pattern: Clear (White)

Formatted: Font color: Black

Formatted: Centered

Deleted: ¶

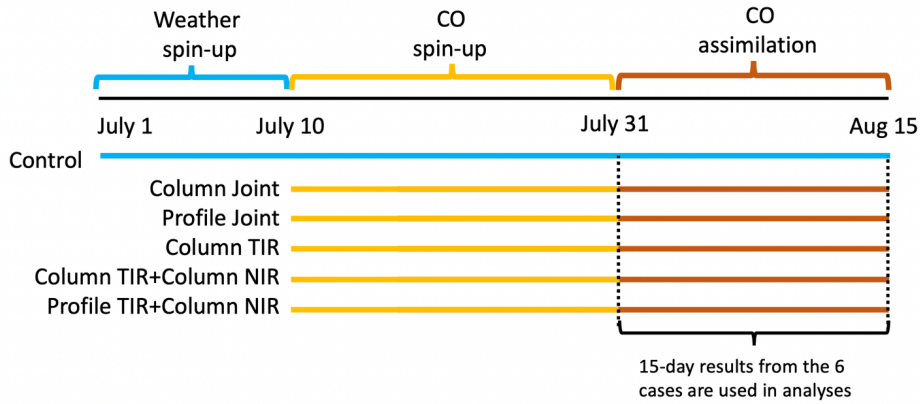




1276  
 1277 **Figure 2.** Daily number of super-observations per day and per grid from MOPITT (a) TIR, (b)  
 1278 NIR, and (c) JNT products during July 16<sup>th</sup> 2018 to August 14<sup>th</sup> 2018. Total Carbon Column  
 1279 Observing Network (TCCON) sites are marked by yellow stars and NOAA Carbon Cycle  
 1280 Greenhouse Gases (CCGG) sites are marked by pink circles.  
 1281

Deleted: 1

1283



1284

1285

1286

1287

1288

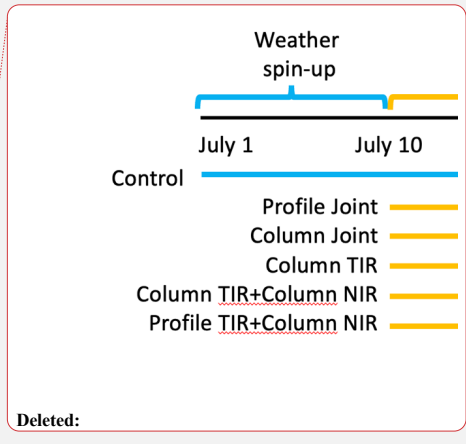
1289

1290

1291

1292

Figure 3. Setup of the CAM-chem/DART data assimilation experiments.



Deleted: 2

Deleted: 2

1293

1294

1295

1296

1297

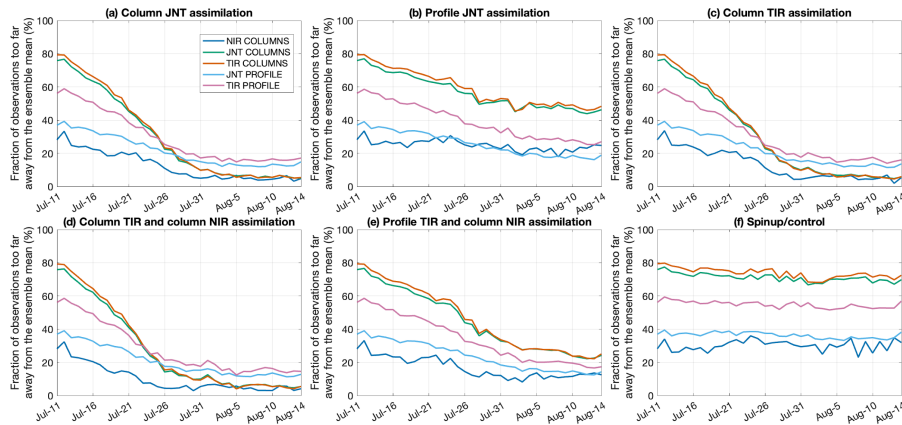
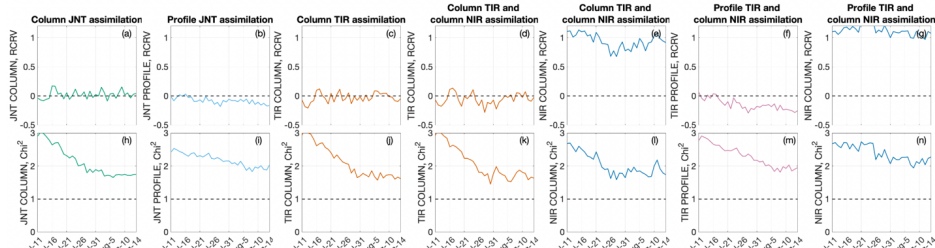


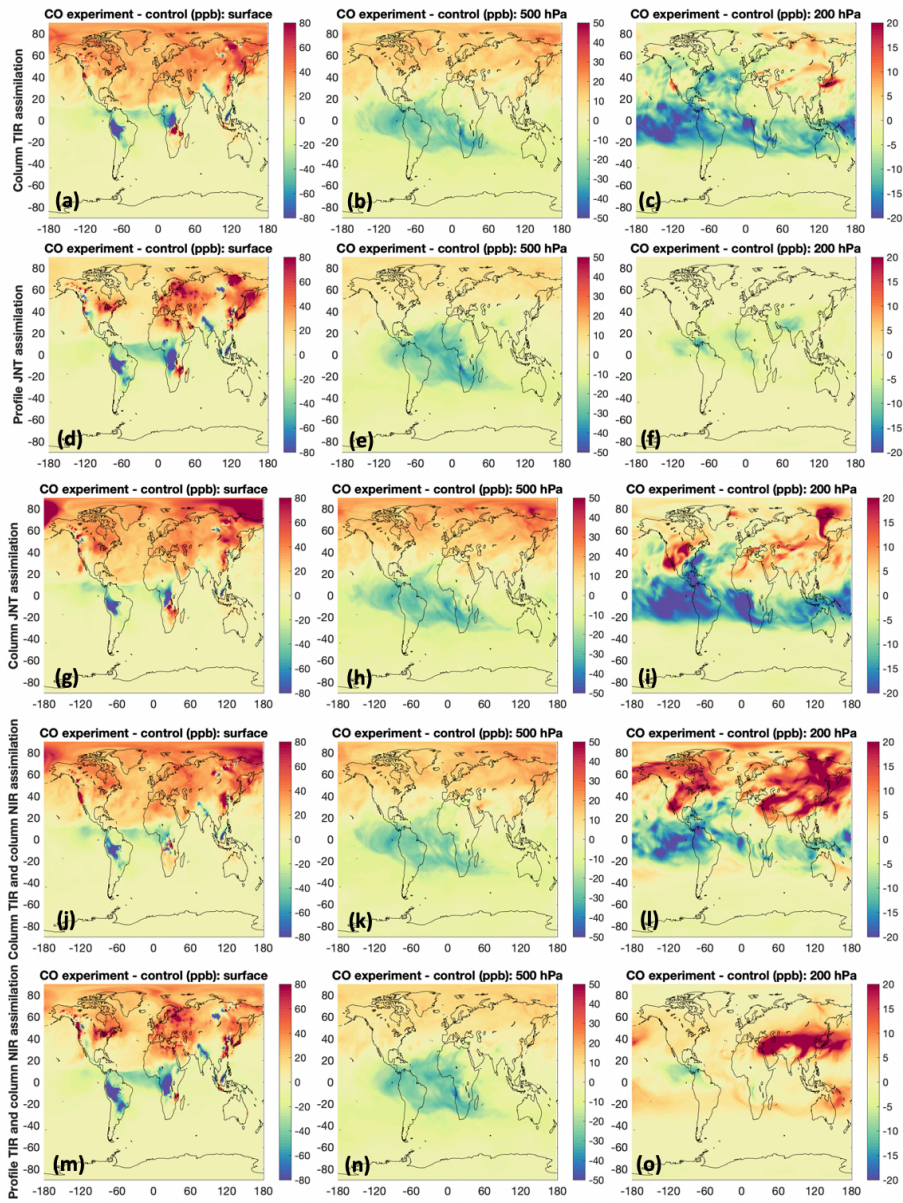
Figure 4. Time series of the fractions of observations rejected by the assimilation system (%) due to that they are too far from the ensemble mean.

Deleted: 3



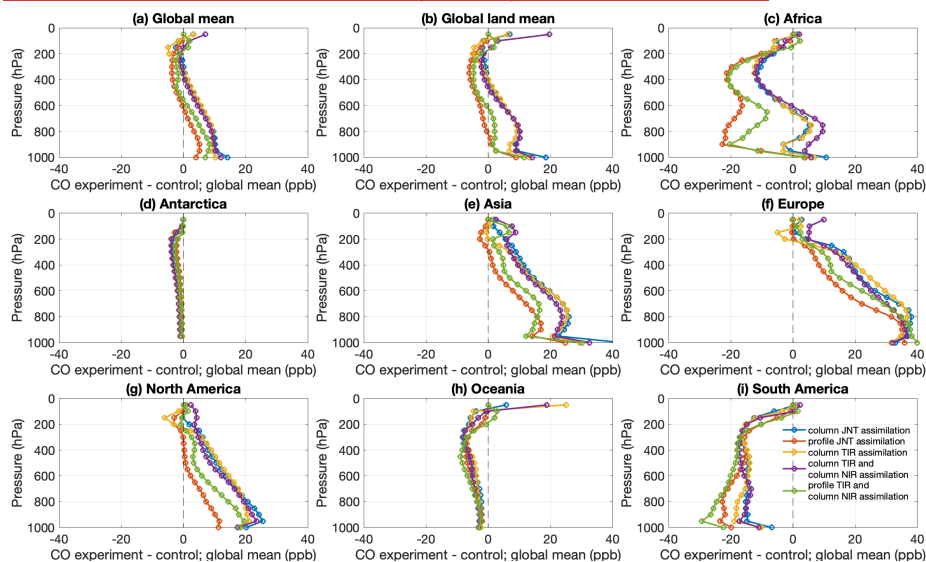
1301  
 1302 **Figure 5.** timeseries of (a-g) daily mean of Reduced Centered Random Variable (RCRV) and (h-  
 1303 n) daily mean of Chi-square. For each experiment, only RCRV and Chi-square of the MOPITT  
 1304 product that were assimilated are shown.  
 1305  
 1306  
 1307

Deleted: 4



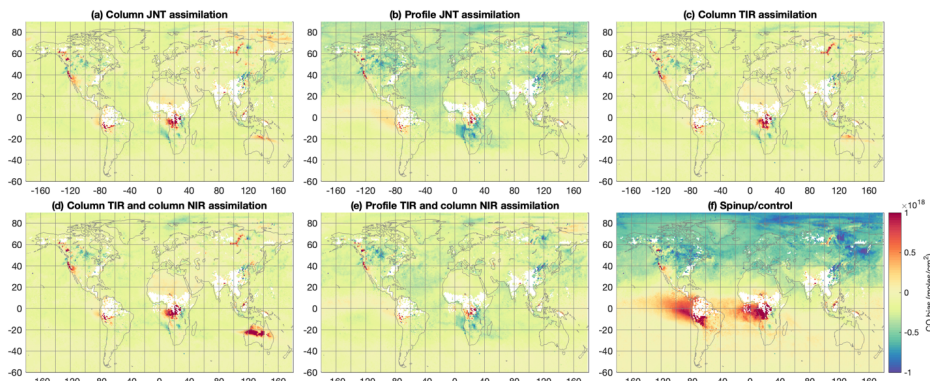
1310 **Figure 6.** 15-day (July 31 - August 14, 2018) average of the difference in CO (forecast of  
 1311 experiment minus control run) for the 5 experiments at the model surface, 500 hPa, and 200 hPa.  
 1312 *Note that the color scales for model surface, 500 hPa, and 200 hPa are different.*

Deleted: 5



1313  
 1314  
 1315 **Figure 7.** Vertical profile of the 15-day (July 31 - August 14, 2018) average difference in CO  
 1316 (forecast of experiment minus control run) over different regions.  
 1317  
 1318

Deleted: 6



1319  
 1320 **Figure 8.** 15-day (July 31 - August 14, 2018) mean biases (ppb) of modeled CO against CO  
 1321 columns from the TROPOspheric Monitoring Instrument (TROPOMI) for the 5 experiments and  
 1322 the control run. TROPOMI averaging kernels are applied to model CO for the comparisons.  
 1323

Deleted: 7

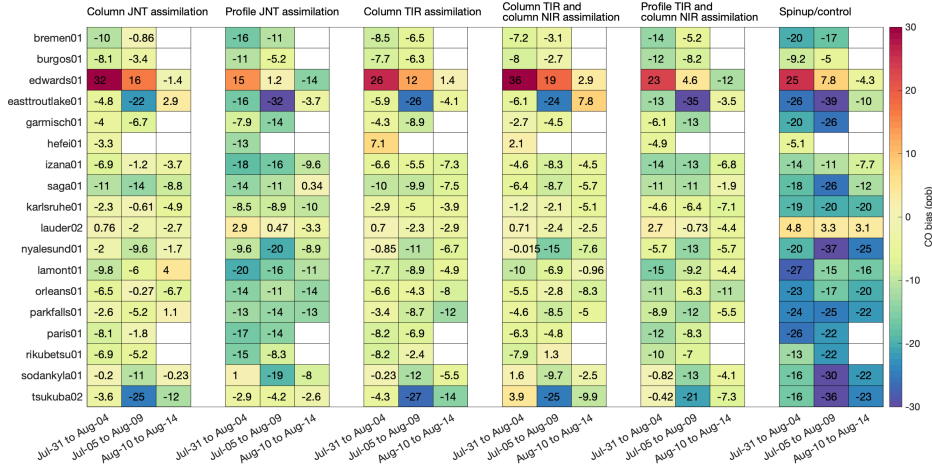
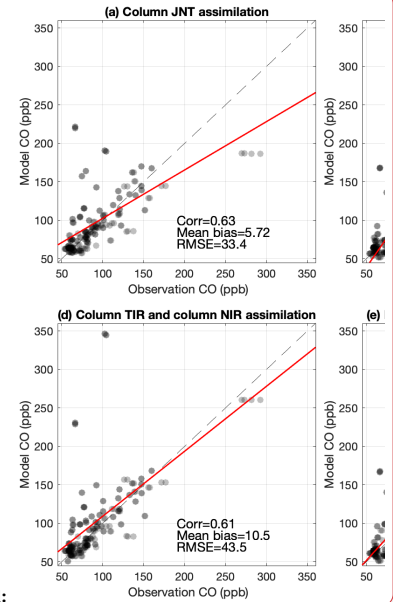


**Figure 9.** Mean biases (ppb) of modeled CO against CO columns from the Total Carbon Column Observing Network (TCCON) for the 5 experiment and the control run. TCCON averaging kernels are applied to model CO for the comparisons. Spatial locations of TCCON sites can be found in Figure 3, and Figure S1. A time series of TCCON and modeled CO can be found in Figure S4.

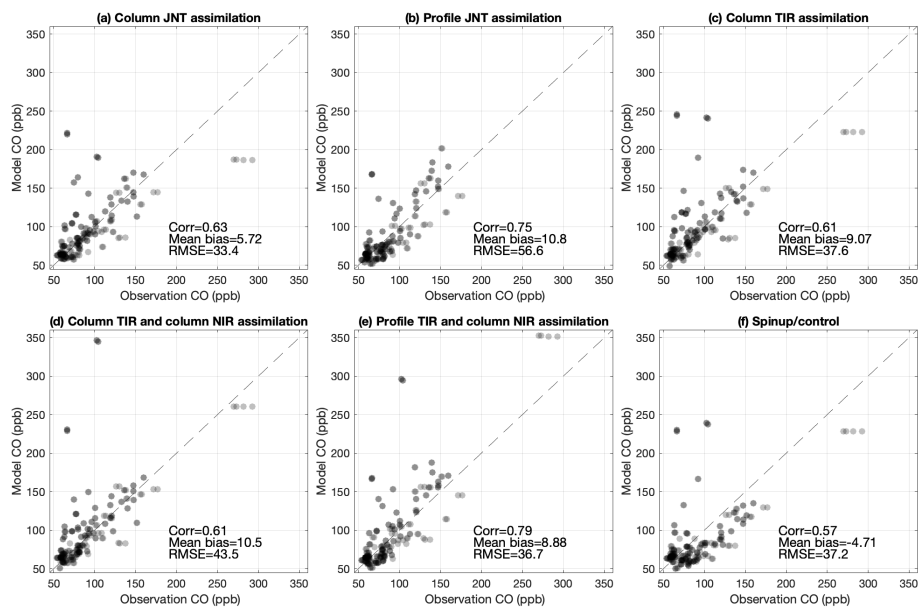
1328  
 1329  
 1330  
 1331  
 1332  
 1333  
 1334  
 1335  
 1336  
 1337

Deleted: 8

Deleted: 2



Deleted:



1341  
 1342 **Figure 10.** Comparisons of modeled CO (ppb) and CO observations (ppb) from the NOAA Carbon  
 1343 Cycle Greenhouse Gases (CCGG) sites during July 31st, 2018 to August 14th, 2018 for the 5  
 1344 experiments and the control run. Spatial locations of CCGG sites can be found in Figure 3, and  
 1345 Figure S1. A spatial distribution of model bias in CO against CO observations from CCGG sites  
 1346 can be found in Figure S5.  
 1347  
 1348

Deleted: 9  
 Deleted: 2

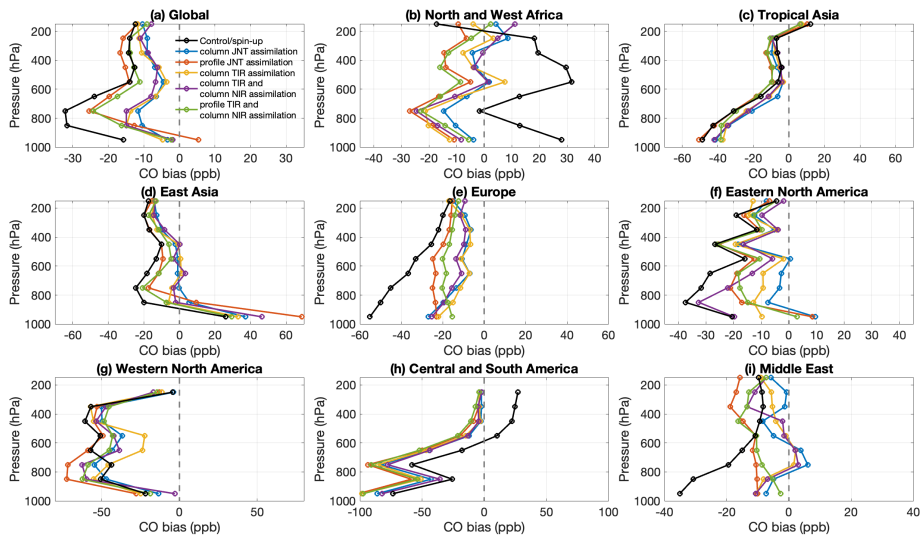


**Figure 11.** Mean biases (ppb) of modeled CO against CO profiles from the In-service Aircraft for a Global Observing System (IAGOS) measurements for the 5 experiments (colored lines) and the control run (black line) at different vertical levels. Locations of IAGOS CO profiles can be found in Figure S2.

Deleted: 0

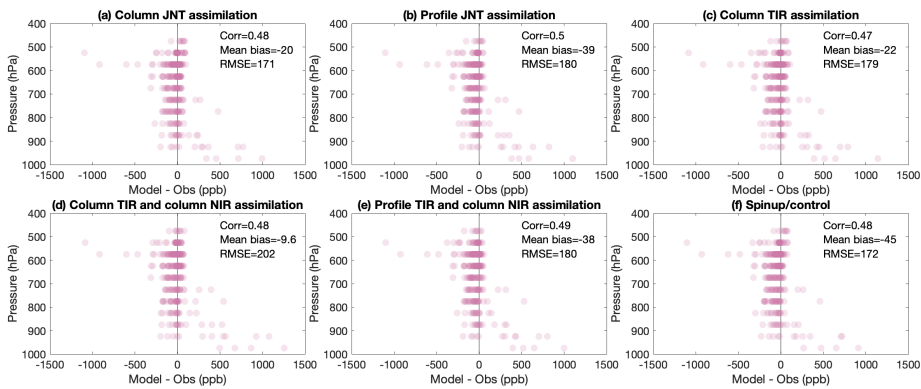


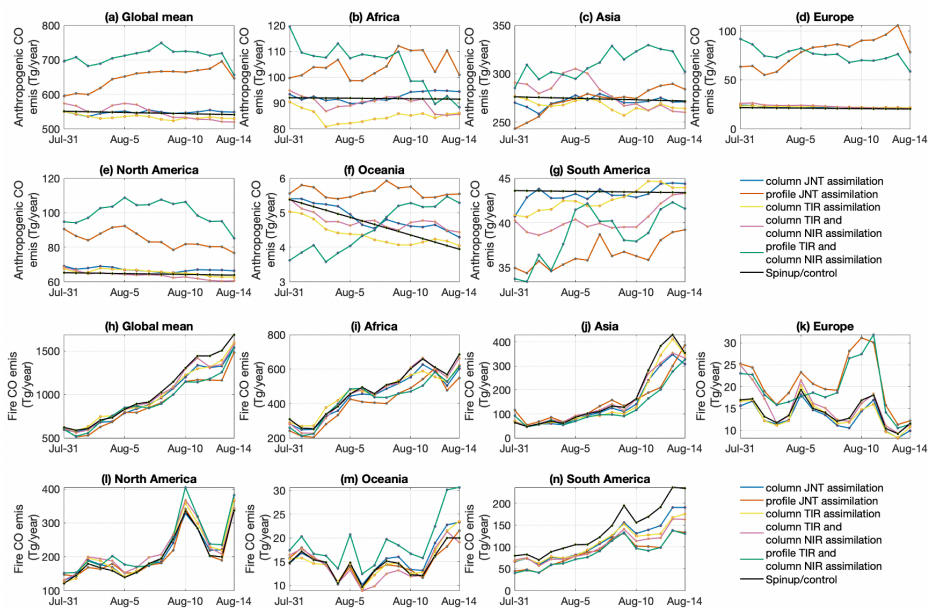
**Figure 12.** Mean biases (ppb) of modeled CO against airborne CO observations from the Western wildfire Experiment for Cloud chemistry, Aerosol absorption and Nitrogen (WE-CAN) field campaign for the 5 experiments and the control run at different vertical levels.

Deleted: 1

1351  
1352  
1353  
1354  
1355  
1356  
1357

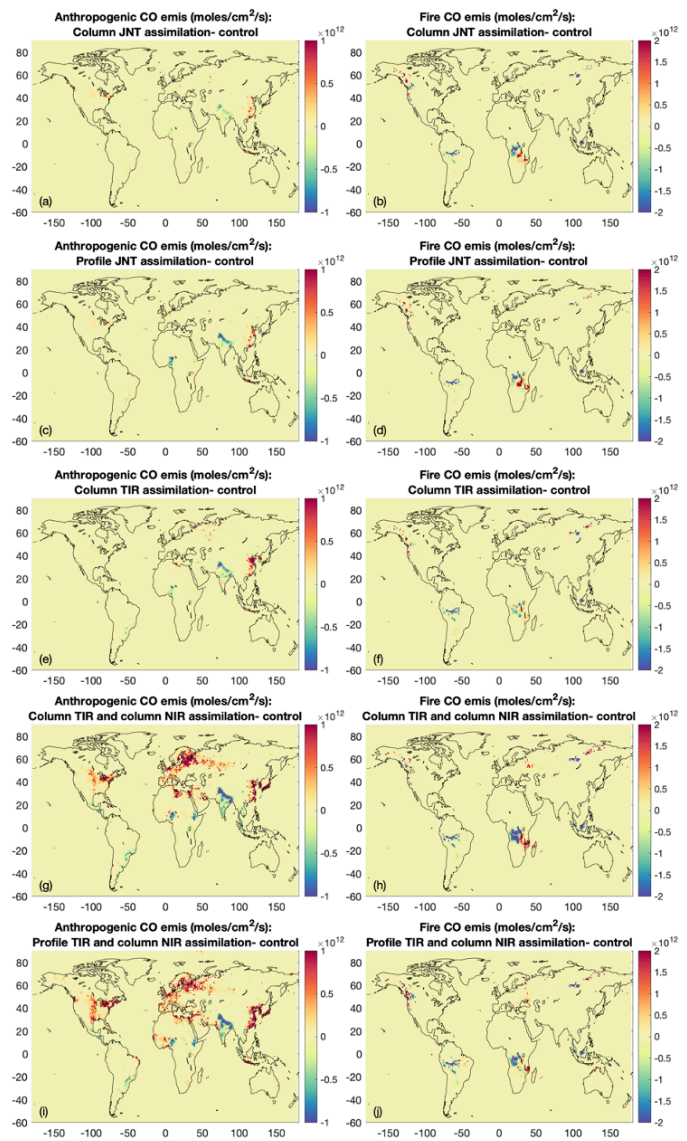
1358  
1359  
1360  
1361  
1362  
1363





1366  
 1367 **Figure 13.** Updated (a-g) CAMS anthropogenic CO emissions and (h-n) FINNv2.4 fire CO  
 1368 emissions as a result of assimilating different MOPITT products. The emissions from the  
 1369 Spinup/control run are the unchanged original emissions of CAMS and FINNv2.4.

Deleted: 2



1371  
 1372 **Figure 14.** Updates on the (a) CAMS anthropogenic CO emissions and (b) FINNv2.4 fire CO  
 1373 emissions as a result of assimilating MOPITT Column JNT product. Updates is calculated as CO  
 1374 from the experiment minus CO from the control run. (c-j) are similar to (a-b) but for other  
 1375 experiments.

Deleted: 3